GEORG-AUGUST-UNIVERSITÄT
GÖTTINGEN

Fakultät für
Physik

**Bachelor's Thesis**

# Analyse von $pp \to t\bar{t}H$ Ereignissen

# Analysis of $pp \to t\bar{t}H$ Events

prepared by

**Felix Wiebe**

from Siegburg

at the II. Physikalischen Institut

**Thesis number:** II.Physik-UniGö-BSc-2014/05

**Thesis period:** 14th April 2014 until 20th July 2014

**First referee:** Prof. Dr. Arnulf Quadt

**Second referee:** PD Dr. Kevin Kröninger

# Contents

# 1 Introduction

Humankind always has been interested in the constituents that matter is made of. Already ancient Greek philosophers had the idea that matter is built of small particles which they called atoms (gr. $\alpha\tau o\mu o\varsigma$ indivisible), that can not be divided further.
Today, atoms have been split and the smallest particles in our theory are the elementary particles of the Standard Model of particle physics. The Standard Model is the most fundamental and accurate theory we have and so far it is very successful.
Modern particle physicists collide particles at very high speeds to discover new physics at smallest length scales. This is only possible with very high energies. Therefore, particle accelerators such as the LHC which currently is the largest and most powerful particle accelerator, are needed. The LHC can collide protons at center of mass energies of $\sqrt{s} = 7\,\text{TeV}$ up to maybe $\sqrt{s} = 14\,\text{TeV}$ next year. One main purpose of the LHC is to find the Higgs boson, which has been discovered in 2012, and to study its properties. Also there might be physics beyond the Standard Model like supersymetric particles that might be found at the LHC.
Theoretical predictions on this level are very difficult because in most cases the equations of motion are not analytically solvable. Instead, computer simulations are used to compare measured data with theory. Of course there are many different ways and models to simulate these interactions on a fundamental level. The goal of this bachelor thesis is to compare some of them. Analysed are the event generators PowHel [1] and aMC@NLO [2], the parton shower and hadronisation models PYTHIA 8 [3] and HERWIG++ [4] as well as Madspin [5], a program to decay unstable particles.
The analysed event channel is $pp \to t\bar{t}H$, in which the coupling of the Higgs boson to b quarks can be studied.

Chapter 2 introduces the fundamentals of the Standard Model and hadron collider physics. Additionally there is an extra section about the $t\bar{t}H$ process. The next chapter 3 explains briefly Monte Carlo generations and the simulation models that are used in this thesis. Chapter 4 focuses on the production of datasets and in chapter 5 the results of the comparison of these datasets are explained. Chapter 6 is a conclusion.

# 2 Theoretical Framework

This chapter contains a brief overview over the Standard Model, an introduction into hadron collider physics and the last section focuses on $t\bar{t}H$ events which are studied in this thesis.

## 2.1 The Standard Model of Particle Physics

The Standard Model is a very successful theory which has been tested by a lot of experiments. This section gives a short overview of the Standard Model with special emphasis on the top quark and the Higgs boson. See reference [6] for a more detailed explanation. In this thesis, all quantities are expressed in natural units with $\hbar = c = 1$.

### 2.1.1 Elementary Particles

The smallest constituents, that matter consists of, are elementary particles. They are indivisible and assumed to be point-like. An elementary particle is characterized by its mass, electric charge, colour and spin. The current Standard Model contains 61 different particles. The particles are classified in two types. There are bosons with integer spins and fermions with half integer spins.
Out of the 61 particles, 48 are fermions with spin 1/2. There are six types of quarks (u, d, c, s, t, b) and six types of leptons ($\nu_e$, $e^-$, $\nu_\mu$, $\mu^-$, $\nu_\tau$, $\tau^-$) . Each quark can carry one of the three colours red, blue and green. Colour carrying particles are never observed individually because they form colourless bound states with other particles. Particles that are build of quarks are called hadrons.
Additionally each of these fermions has an anti-particle with the opposite charge and colour. Pairing the fermions with their weak isospin partner yields three generations, which are listed in figure 2.1. In the figure also the masses and electrical charges of all particles can be found.
The remaining 13 particles are bosons. With one exception, they are vector bosons with spin 1 and mediate interactions between elementary particles. The Standard Model describes the electromagnetic force (mediator: photon,$\gamma$), the weak force ($W^\pm$, $Z^0$) and the

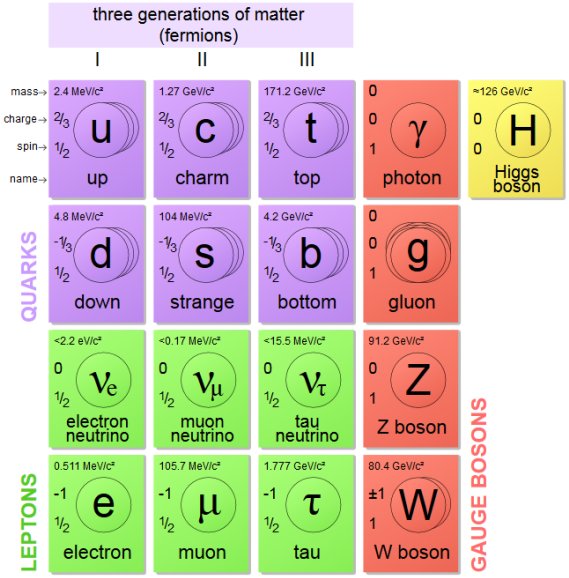


***Figure 2.1:*** Illustration of the three particle generations, gauge bosons and the Higgs boson. In the boxes also the masses, electrical charge and spin of the particles are listed.

strong force (eight gluons, g). The last remaining particle is a scalar boson, the Higgs boson, which is discussed in detail in section 2.1.3.

### 2.1.2 Top Quark

The top quark was predicted by Kobayashi and Maskawa in 1973 and was discovered in 1995 at the TEVATRON collider at FERMILAB. The experiments CDF and DØ jointly announced the discovery of the top quark [7], [8].
The top quark with a mass of $m_t = (173.34 \pm 0.27(\text{stat}) \pm 0.71(\text{syst}))\,\text{GeV}$ [9] is the heaviest known elementary particle. The top quark is a very interesting particle to study because it is the only quark that decays before it forms bound states.

#### Production

A top quark is produced either via the strong interaction as a $t\bar{t}$ pair or via the weak interaction as a single top quark. The Feynman diagrams for the $t\bar{t}$ pair production at leading order (LO) are shown in figure 2.2.

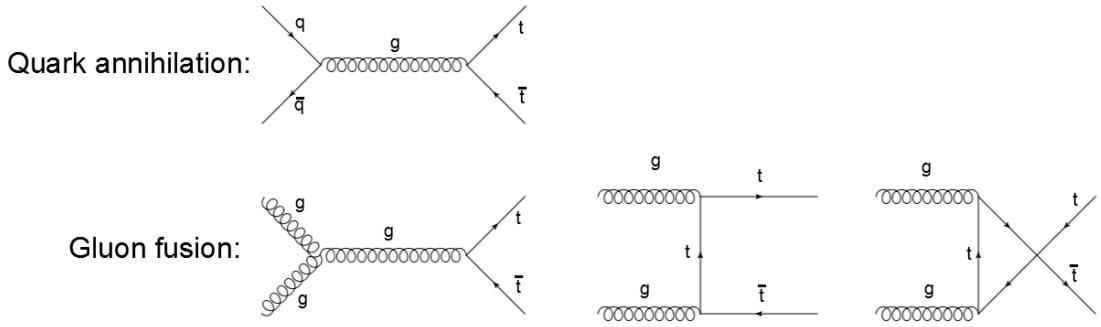


***Figure 2.2:*** LO Feynman diagrams of the production of $t\bar{t}$ pairs at the LHC.

### Decay

In theory, the top quark has a decay width of $\Gamma = 1.33\,\text{GeV}$ [10] and has therefore a very short lifetime of $\tau \approx 5 \cdot 10^{-25}\,\text{s}$ [11], which is shorter than the time scale on which quarks form bound states ($\sim 10^{-22}\,\text{s}$). So the top quark is the only quark which can be studied as a free particle.
The top quark almost exclusively decays into a $b$ quark and a $W^+$ boson. The anti top quark decays analogically into a $\bar{b}$ quark and a $W^-$ boson.

## 2.1.3 Higgs Boson

The Higgs boson was predicted by Peter Higgs in 1964 [12] and its discovery at the LHC at CERN was announced by ATLAS and CMS on the 4th of July 2012 [13],[14].
The Higgs boson has a mass of around $m_H \approx 125\,\text{GeV}$ [15]. The coupling strength of the Higgs boson to another particle scales with the mass of the particle it interacts with. The higher a particle mass is, the stronger is the coupling of the Higgs boson to it.

### Production

The Feynman diagrams of the four dominant production processes are shown in figure 2.3. The dominant contribution to the production of Higgs bosons at the LHC is gluon fusion. It also can be produced by quark annihilation but this is less likely at high energies. Furthermore a Higgs boson can be radiated off by a $W$, $Z$ or top quark.

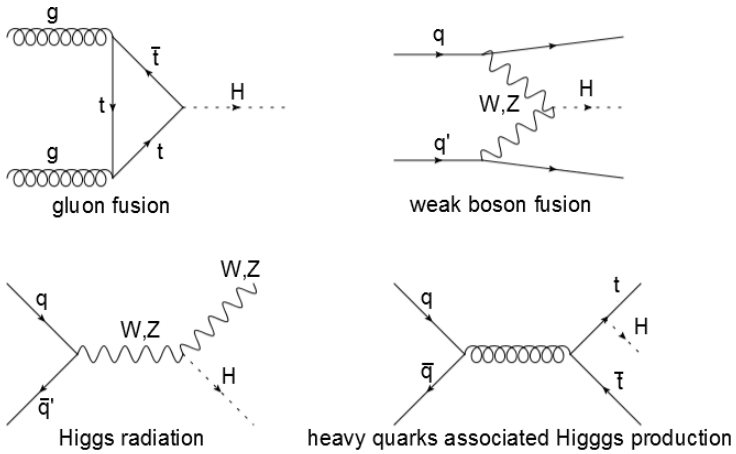


***Figure 2.3:*** The four dominant production processes of Higgs bosons at the LHC.

**Decay**

The Standard Model predicts a lifetime of $\tau = 1.56^{-22}\,\mathrm{s}$ [16] for the Higgs boson. It is confirmed that it can decay into a $W$ pair, a $Z$ pair and two photons. But the most likely decay as predicted in the Standard Model is $H \to b\bar{b}$ with a branching ratio of 0.578. Table 2.1 lists the branching ratios of all possible decays of the Higgs boson within the Standard Model. The values are taken from NLO theoretical calculations.

| Decay channel | Branching ratio |
|---|---|
| $H \to b\bar{b}$ | $5.78 \cdot 10^{-1}$ |
| $H \to WW$ | $2.16 \cdot 10^{-1}$ |
| $H \to gg$ | $8.56 \cdot 10^{-2}$ |
| $H \to \tau^-\tau^+$ | $6.37 \cdot 10^{-2}$ |
| $H \to c\bar{c}$ | $2.68 \cdot 10^{-2}$ |
| $H \to ZZ$ | $2.67 \cdot 10^{-2}$ |
| $H \to \gamma\gamma$ | $2.30 \cdot 10^{-3}$ |
| $H \to Z\gamma$ | $1.55 \cdot 10^{-3}$ |
| $H \to s\bar{s}$ | $4.40 \cdot 10^{-4}$ |
| $H \to \mu\bar{\mu}$ | $2.21 \cdot 10^{-4}$ |
| $H \to t\bar{t}$ | 0.00 |

***Table 2.1:*** Theoretical NLO branching ratios of the possible Higgs decays [17].

### 2.1.4 Interactions

There are three different kinds of interactions between particles in the Standard Model: the electromagnetic, the weak and the strong force. By demanding invariance of the Lagrangian under local gauge transformations the forces are included in the theory in a

natural way.
The behaviour of a particle field $\psi$ can be described by a Lagrangian $\mathcal{L}(\psi, \dot{\psi})$. A spin $\frac{1}{2}$ particle with mass $m$ for example is described by the Dirac Lagrangian density

$$\mathcal{L} = i\hbar c\bar{\psi}\gamma^\mu\partial_\mu\psi - mc^2\bar{\psi}\psi \tag{2.1}$$

Now one can perform a local gauge transformation $\psi \to e^{i\theta(x)}\psi$ (analog: $\bar{\psi} \to e^{-i\theta(x)}\bar{\psi}$) of the field. By doing so the Lagrangian picks up an additional term from the derivative of $\theta$. To get rid of that, one introduces a new field, $A_\mu$, in the Lagrangian which transforms under gauge transformations as follows $A_\mu \to A_\mu - \frac{\hbar c}{q}\partial_\mu\theta$. The Lagrangian

$$\mathcal{L} = i\hbar c\bar{\psi}\gamma^\mu\partial_\mu\psi - mc^2\bar{\psi}\psi - (q\bar{\psi}\gamma^\mu\psi)A_\mu \tag{2.2}$$

is now invariant. The last term describes the interaction of $\psi$ and the new gauge field $A_\mu$. But there is no description of the propagation of the field $A_\mu$. $A_\mu$ is a vector field which is described by the Proca Lagrangian for spin 1 particles:

$$\mathcal{L} = \frac{-1}{16\pi}F^{\mu\nu}F_{\mu\nu} + \frac{1}{8\pi}\left(\frac{m_A c}{\hbar}\right)^2 A^\nu A_\nu \tag{2.3}$$

where

$$F^{\mu\nu} = \partial^\mu A^\nu - \partial^\nu A^\mu \tag{2.4}$$

When performing the gauge transformation for $A_\mu$ one sees that the first term in the Lagrangian is invariant whilst the second term is not. So the gauge field has to be massless ($m_A = 0$) and the full Lagrangian reads

$$\mathcal{L} = i\hbar c\bar{\psi}\gamma^\mu\partial_\mu\psi - mc^2\bar{\psi}\psi - (q\bar{\psi}\gamma^\mu\psi)A_\mu - \frac{1}{16\pi}F^{\mu\nu}F_{\mu\nu} \tag{2.5}$$

In fact, here $A_\mu$ is the electromagnetic potential and the Lagrangian describes the interaction of a spin $\frac{1}{2}$ particle with a photon.
By introducing the covariant derivative $\mathcal{D}_\mu = \partial_\mu + i\frac{q}{\hbar c}A_\mu$ one can write the Lagrangian more neatly as:

$$\mathcal{L} = i\hbar c\bar{\psi}\gamma^\mu\mathcal{D}^\mu\psi - \frac{1}{16\pi}F^{\mu\nu}F_{\mu\nu} \tag{2.6}$$

In the example above the factor in the gauge transformation ($e^{i\theta}$) was part of the U(1) group. The full gauge group of the Standard Model is

$$SU(3) \times SU(2) \times U(1) \tag{2.7}$$

If one transforms with elements of the SU(2) group one obtains a description of the weak interaction and the $W^{\pm}$ and $Z$ bosons and transforming with SU(3) yields chromodynamics with its eight gluons. The number of mediating bosons is equal to the degrees of freedom of the gauge group.
The vector bosons obtained by this procedure have to be massless. However, experiments show that the mediators $W^{\pm}$ and $Z$ of the weak force have a mass. This problem is solved by the Higgs mechanism.

### Higgs Mechanism

The principle of the Higgs mechanism is spontaneous symmetry breaking. To understand that principle consider the Lagrangian

$$\mathcal{L} = \frac{1}{2}(\partial_\mu \phi)^*(\partial^\mu \phi) + \frac{1}{2}\mu^2(\phi^*\phi) - \frac{1}{4}\lambda^2(\phi^*\phi)^2 \tag{2.8}$$

where $\phi = \phi_1 + i\phi_2$ is a complex field. Again the Lagrangian is supposed to be locally gauge invariant under the transformation

$$\phi \to e^{i\theta(x)}\phi \tag{2.9}$$

And again this can be obtained by replacing the derivative with a covariant derivative as in equation 2.1.4.
The potential $V$ (see figure 2.4) of the Lagrangian 2.8 has its minimum not at $\phi = 0$ but at

$$(\phi_1^2 + \phi_2^2) = \frac{\mu^2}{\lambda^2} \tag{2.10}$$

which is a circle in the $(\phi_1, \phi_2)$-plane. The field $\phi$ is supposed to be the fluctuation from one of these ground states, which represent the vacuum. So one can define the new fields

$$\eta = \phi_1 - \frac{\mu}{\lambda} \tag{2.11}$$

$$\xi = \phi_2 \tag{2.12}$$

and use the symmetry 2.9 to rotate the $\phi$'s by the angle $\theta = -\arctan(\frac{\phi_2}{\phi 1})$. That yields the new Lagrangian

$$\mathcal{L} = \left(\frac{1}{2}(\partial_\mu \eta)(\partial^\mu \eta) - \mu^2\eta^2\right) + \left(-\frac{1}{16\pi}F^{\mu\nu}F_{\mu\nu} + \frac{1}{2}\left(\frac{q}{\hbar c}\frac{\mu}{\lambda}\right)^2 A_\mu A^\mu\right) \tag{2.13}$$

$$+ \left(\frac{\mu}{\lambda}\left(\frac{q}{\hbar c}\right)^2 \eta A_\mu A^\mu + \frac{1}{2}\left(\frac{q}{\hbar c}\right)^2 \eta^2 A_\mu A^\mu - \lambda\mu\eta^3 - \frac{1}{4}\lambda^2\eta^4\right) + \left(\frac{\mu^2}{2\lambda}\right)^2 \tag{2.14}$$

By picking the rotation angle $\theta$ the field $\xi$ was set to zero. The field $\xi$ described a ghost particle, a so called Goldstone boson. The degree of freedom of the Goldstone boson has been picked up by the gauge field $A_\mu$. As one can see in the second term in the Lagrangian 2.14 the gauge field has acquired a massterm. So in addition to two transverse polarization degrees of freedom the gauge field has one longitudinal one.
Since the gauge field $A_\mu$ now has a mass, it can describe a $W^\pm$ or a $Z$ boson while the field $\eta$ describes the Higgs boson. The third term in the Lagrangian 2.14 describes the coupling of the vector bosons with the Higgs boson and the last term is irrelevant because a constant in the Lagrangian does not contribute to the equations of motion.
Instead of the Lagrangian 2.8 with the two dimensional field $\phi$ one has to use a four dimensional $\phi$ which yields not just one but three gauge fields with mass. These three gauge fields then describe the three mediators of the weak force.

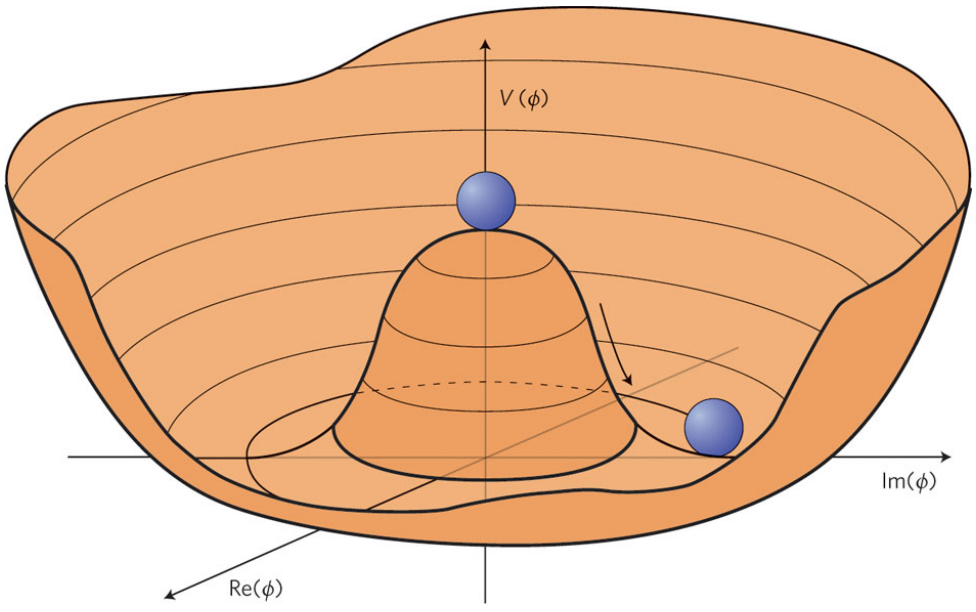


***Figure 2.4:*** The Higgs potential in two dimensions.

## 2.2 Hadron Collider Physics

Hadron collider physics has some difficulties that arise from colliding composited particles instead of elementary particles. For example one does not know the center of mass energy of the original collision because of the momentum distribution of the partons, the constituents of protons.
In this section a short overview of the LHC and one of its experiments, the ATLAS detector, is given. After that, some fundamental concepts of hadron collider physics are explained.

### 2.2.1 LHC

The LHC (**L**arge **H**adron **C**ollider)[18] is the world's largest particle collider. The circumference of the LHC is 27 km. It was built in collaboration with more than 100 countries and is located at the border of Switzerland and France near Geneva at CERN [19]. It started operating in autumn of 2009. In the LHC protons are collided with protons but it is also possible to collide lead atoms with each other. Currently there is data for collisions with center of mass energies of 7 TeV and 8 TeV and the energy will be increased in the next years up to 14 TeV. There are seven detectors at the LHC. The four most important ones are ATLAS, CMS, ALICE and LHCb. The purpose of the LHC is the search for physics beyond the Standard Model and its greatest accomplishment is the discovery of the Higgs boson [**?** ],[14].

### 2.2.2 ATLAS Experiment

ATLAS [20] is one of the main detectors at the LHC. It is a cylindrical multipurpose detector. The following constituents are the most important:

**Inner detector:** The inner tracking detector consists of silicon pixel detectors, silicon strip detectors and a transition radiation tracker. The purpose here is to trace charged particles. By applying a magnetic field and measuring the curvature of a particle it is also possible to calculate the momentum of passing particles.

**Calorimeters:** There are two kinds of calorimeters. The electromagnetic calorimeter (ECAL) and the hadronic calorimeter (HCAL). To measure the energy of passing particles, the particles are supposed to deposit their whole energy in the calorimeters. The calorimeters basically consist of massive matter with some detecting layers in between.

Electrons, positrons and photons create via pair production and Bremsstrahlung showers in the ECAL. In the HCAL hadrons collide inelastically with the nuclei in the HCAL.

**Muon spectrometer:** The muon chambers detect the only charged particles that survived the calorimeters, which are muons.

### 2.2.3 Kinematics

The obvious choice for a coordinate system in a detector are cylindrical coordinates with the origin at the interaction point. The z-axis is aligned to the beam pipe. $\phi$ is the azimuthal angle around the beam pipe and $r$ the radial distance.
Usually the momentum of the colliding particles in z direction is unknown. For this reason one usually works with transversal quantities. The transversal momentum and transversal energy are defined as

$$p_T = \sqrt{p_x^2 + p_y^2} \tag{2.15}$$

$$E_T = E \sin\theta \tag{2.16}$$

The transverse mass of a system with two particles of which one cannot be detected directly is

$$m_T^2 = (E_{T,1} + E_{T,2})^2 - (p_{T,1} + p_{T,2})^2 \tag{2.17}$$

The pseudorapidity of a particle is defined as follows

$$\eta = -\ln(\tan(\theta/2)) \tag{2.18}$$

where $\theta$ is the polar angle of the particle to the beam pipe.
Neutrinos are not detected in the detector. Also there might be physics beyond the Standard Model which is not detected. But by energy and momentum conservation one can predict the total transverse energy and momentum of the final state particles and so it is possible to reconstruct energy and momentum of a neutrino, if there is only one in the event. So often it is important to look for missing transverse energy and momentum.

### 2.2.4 Proton Collisions

The LHC collides protons with protons. In reality such collisions are not as clean as Feynman diagrams suggest sometimes. Figure 2.5 illustrates the complexity and the

most important processes that happen during a *pp* collision.
Even before the collision the protons can radiate off gluons and photons. This process is called initial state radiation.
The hard process of a collision is the actual event which will be analysed later.
The new particles, that were created in the event, again can radiate off gluons or photons which in that case is called final state radiation.
After that the hadronisation happens. Particles that carry a colour are never observed separately. They form colourless bound states in a process that is called hadronisation. These colourless bound states then can be detected as jets.
But during such a proton collision not just one interaction takes place. The less energetic interactions are called underlying event.

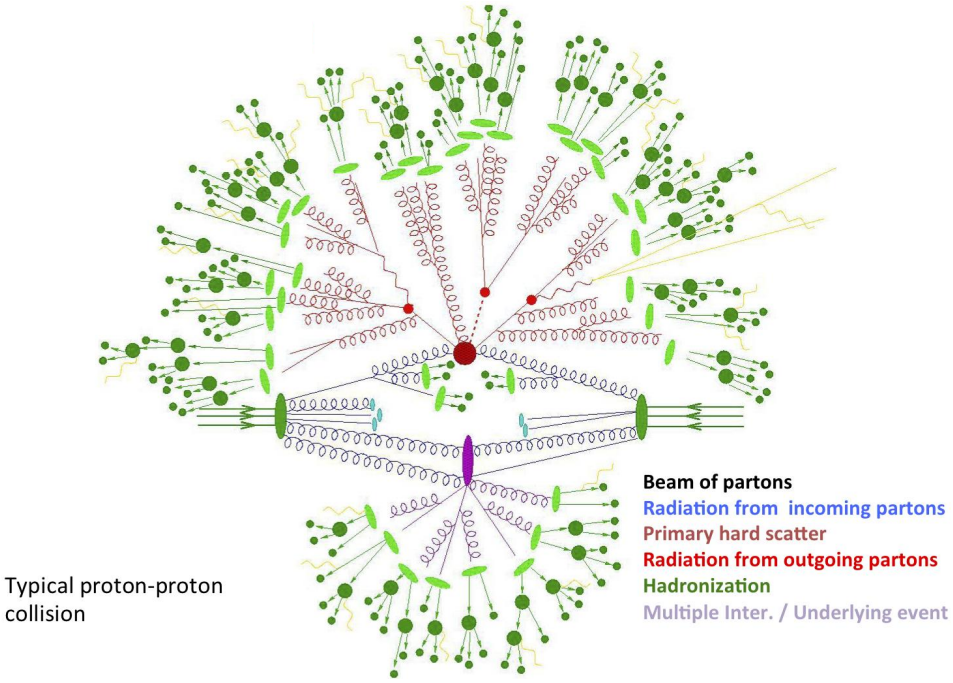


***Figure 2.5:*** Illustration of a *pp* collision.

### Parton Distribution Functions

The proton is not an elementary particle because it has a substructure. It is composed of so called partons which are quarks and gluons. In the easiest case, when looking at the proton at low energies, it consists of three quarks (uud) and each of the quarks carries one third of the total proton momentum. But with increasing energy the gluons and sea quarks gain importance in the reaction. The fraction of the total proton momentum of

each particle is called Bjorken-$x$. A parton distribution function (PDF) is a function of the Bjorken-$x$ that gives the probability of finding a parton of an specific $x$. In figure 2.6 the PDF of a proton is shown.

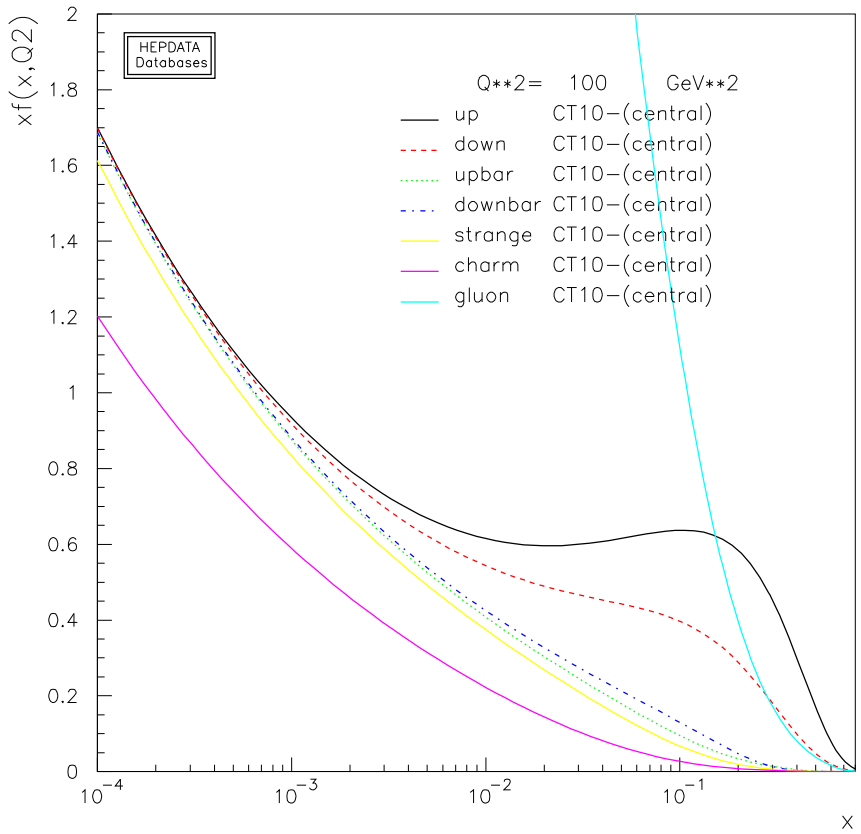


***Figure 2.6:*** PDF of a proton. On the x-axis is the Bjorken-$x$ and on the y-axis the momentum distribution function $f$ times $x$.

### Cross Sections of Hadronic Collisions

In figure 2.7 the cross section of $pp$ interactions is compared to cross sections of various hadronic processes. The interaction with photons can be interpreted as a hadronic interaction by assuming that the photons create pairs of quarks in form of mesons, which can interact strongly.

While the cross section of $p\bar{p}$ processes is bigger at low energies the cross section of $pp$ interactions and $p\bar{p}$ interactions approach each other with increasing energy. The reason is that with increasing energy the contribution of sea quarks increases and the composition of protons or anti protons matters less.

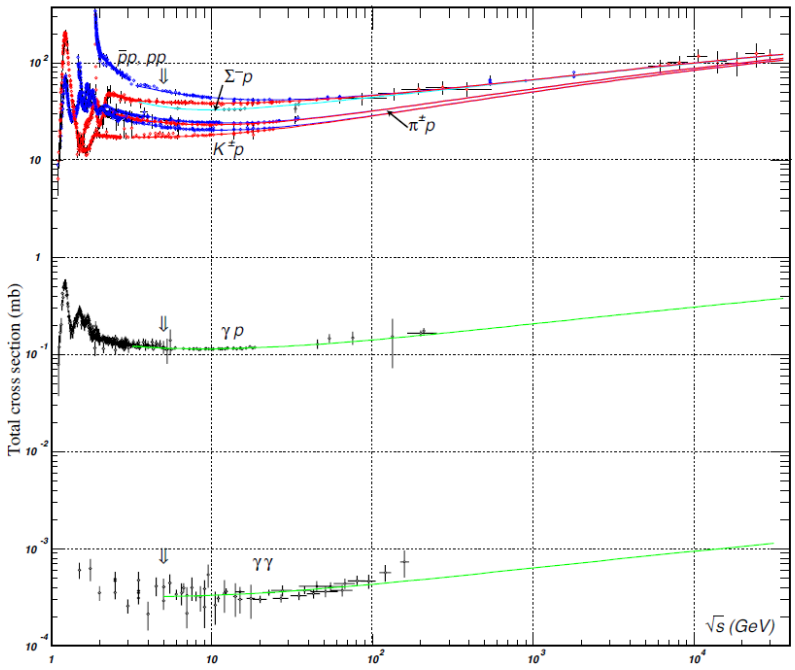


***Figure 2.7:*** Comparison of hadronic cross sections plotted against the cms energy [10].

The cross section of two colliding hadrons $a$ and $b$ is

$$\sigma = \sum_{a,b} \int \mathrm{d}x_1 \mathrm{d}x_2 f_a(x_1, \mu_F) f_b(x_2, \mu_F) \hat{\sigma}(x_1, x_2, \mu_R) \tag{2.19}$$

where $f_a(x_1, \mu_F)$ and $f_b(x_2, \mu_F)$ denote the PDF's of the hadrons and $\hat{\sigma}(x_1, x_2, \mu_R)$ is the hadronic cross section. The factors $\mu_F$ and $\mu_R$ are the factorisation scale and the renormalisation scale.

**Factorisation scale:** The factorisation theorem states that it is possible to divide the PDF's in the calculation of the cross section into a long distance term and a short distance term. Since the higher orders have been separated from the short distance term it is now of finite order and can be calculated with perturbative QCD. The long distance terms are soft processes. The factorisation scale $\mu_F$ is the boundary between the short and long distance part.

**Renormalisation scale:** The contributions of loop diagrams to the propagation of colour carrying particles diverge to infinity. This infinity is absorbed in the strong force. That means that the strong coupling constant depends on the distance to the charge. The energy corresponding to the distance is called renormalisation scale $\mu_R$.

Although it would be possible to choose different values for the renormalisation scale and the factorisation scale, in Monte Carlo simulations it is common to set these scales equal $\mu_R = \mu_F$.
The scales can be set either static or dynamic. A static scale would be for example the sum of the transverse masses of the particles created in the hard process. A dynamic scale means that it changes per event depending on the different transverse momenta of the final state particles.

## 2.3 $t\bar{t}H$ Process

A $t\bar{t}$ pair and a Higgs boson can be produced either by the interaction of two quarks or by the fusion of two gluons. The Feynman diagram in figure 2.8 illustrates such an event. In this thesis always the $H \rightarrow b\bar{b}$ decay mode is studied.

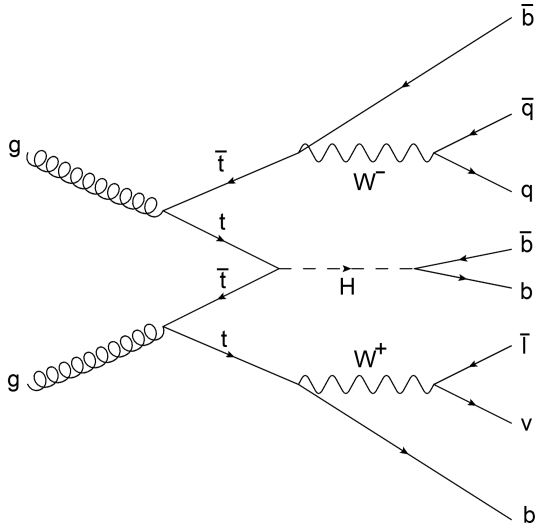


***Figure 2.8:*** Feynman diagram of a $t\bar{t}H$ event ($\ell + jets$ channel).

### 2.3.1 $t\bar{t}H$ Topology ($H \rightarrow b\bar{b}$)

Because of the short lifetime of top quarks, they decay immediately into a b quark and a $W$ boson. Therefore, the topology of a $t\bar{t}H$ event is determined not just by the decay of the Higgs boson but also by the decay of the $W$ bosons. A $W$ boson can decay either in two quarks or two leptons. So besides the four jets of the $b$ quarks from the Higgs boson and the (anti) top quarks there are zero, two or four additional jets originating from the $W$ bosons.

- The decay channel, in which both $W$ bosons decay into leptons, is called **dilepton channel**. In this channel there are two jets from the $b$ quarks and two tracks of charged leptons. In addition two neutrinos are created whose energy is not measured. This channel has a branching ratio of about 5%.

- In the **lepton + jets channel** one $W$ boson decays leptonically and the other one decays hadronically. Hence, in the detector four jets and the track of one charged lepton can be seen and one neutrino escapes the detector. The branching ratio of this channel is about 30%. A decay into a $\tau$ and a neutrino often is not counted in this channel because a $\tau$ can cause jets in the detector as well.

- If both $W$ bosons decay into quarks, the channel is called **all hadronic channel** and one can observe six jets in addition to the Higgs decay products. In this case it is very difficult to reconstruct the original event.
  Figure 2.9 is an overview of the decay channels.

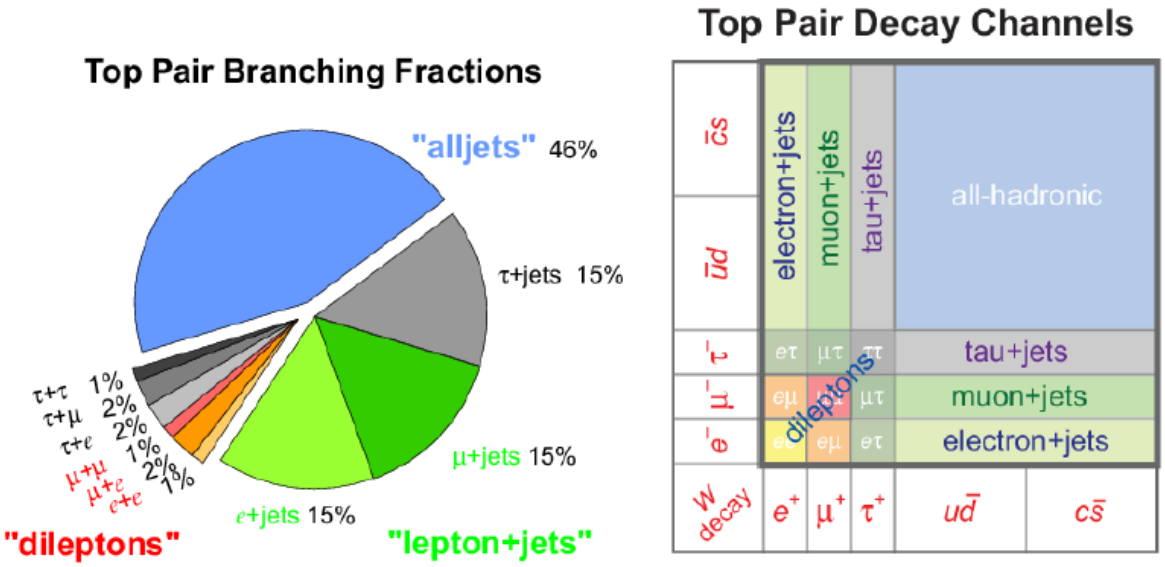


***Figure 2.9:*** Overview over the decay products of $t\bar{t}$ events.

### 2.3.2 $\ell +$ *jets* channel

In the samples simulated in this work the $\ell +$ *jets* channel has been selected. In comparison to the dilepton channel this channel has the advantage that only one neutrino is

created and its energy and momentum therefore can be reconstructed. On the other hand this channel has two jets less than the all hadronic channel. So the $\ell + jets$ channel seems to be a good compromise.

### 2.3.3 Background

The background of the $t\bar{t}H$ channel depends of the decay of the Higgs boson. If the Higgs boson decays into two $b$ quarks the main background is: $pp \to t\bar{t}jj$.
With the two $b$ quarks from the Higgs boson, there are in total four $b$ quarks in the final state. If the b-tagging is working properly, one can reduce the $t\bar{t}jj$ background. The remaining background $t\bar{t}b\bar{b}$ is called irreducible background.
In table 2.2 you can see the cross section of $t\bar{t}H$ events and the cross sections of the background events at $\sqrt{s} = 8\,\text{TeV}$. The cross section of $t\bar{t}H$ events is very small in comparison to the background. So it is very difficult to analyse this channel and it is important to model it properly.

| Decay channel | Cross section [pb] |
|---|---|
| $t\bar{t}H$ | $0.1302 \pm 0.02$ [21] |
| $t\bar{t}jj$ | $20.97 \pm 0.03$ [22] |
| $t\bar{t}b\bar{b}$ | $0.2293 \pm 0.0003$ [22] |

***Table 2.2:*** NLO cross sections of the $t\bar{t}H$ channel and its backgrounds at $\sqrt{s} = 8\,\text{TeV}$. The background cross sections are obtained with Monte Carlo generation.

#### b-tagging

In most events there is more than one jet involved and it is important to reconstruct which jet belongs to which particle. The $b$ quark has a long enough average lifetime to travel a few millimeters after its production in the beam pipe. The particles the $b$ quark decays into therefore do not originate from the beam line but from a slightly shifted point. This point, where the $b$ quark decays, is called secondary vertex. By tracing the particles within the jets one can distinguish between particles that come from the primary vertex and particles that come from a secondary vertex. With this technique it is possible to find out if there was a $b$ quark involved in the interaction and if so to assign the right jet to it.

# 3 Monte Carlo Simulations

Theoretical predictions for the collisions of particles at high energies are not trivial. In most cases it is not possible to solve the equations of motion analytically. Instead Monte Carlo generators are used to solve the equations for the needed quantities numerically.
In the process of generating a proton-proton collision event one has to simulate various steps. For each of these steps different kinds of simulators are used. In this chapter, after an explanation of the general principle, these steps and generators are introduced.

## 3.1 General Principle

In particle physics one often has to integrate over a probability density to obtain a measurable quantity. Suppose, for example the decay of a particle 1 into two other particles 2 and 3. The decay rate then is given by [6]:

$$\Gamma = \frac{S}{\hbar m_1}\left(\frac{c}{4\pi}\right)^2 \frac{1}{2}\int \frac{|\mathcal{M}|^2}{E_2 E_3}\delta^4(p_1 - p_2 - p_3)\,\mathrm{d}^3\vec{p}_2\,\mathrm{d}^3\vec{p}_3 \tag{3.1}$$

The masses of the particles are indicated by $m$, their energies by $E$ and their (four-) momenta by $p$. The $\delta$-function ensures energy and momentum conservation. $S$ is a combinatorial factor $\frac{1}{j!}$ for $j$ identical particles in the final state. The square of the matrix element $|\mathcal{M}|^2$ is the probability density here and the integration goes over the phase space of the final state particles.
In most cases the phase space has many dimensions and integrals like 3.1 are too difficult to be evaluated analytically. Instead numerical methods are used.
In the following the basic principle of Monte Carlo methods is explained. Consider an integral

$$I = \int_{x_1}^{x_2} f(x)\mathrm{d}x \tag{3.2}$$

over an non-negative function $f(x)$ with a maximum $f_{max}$ in the interval $(x_1, x_2)$. The key ingredient for Monte Carlo methods are random numbers $R$. First one chooses a random

number $x_{rand}$ in the allowed x-interval. Then one chooses another random number $y_{rand}$ between 0 and $f_{max}$. One now has to check if $y_{rand} < f(x_{rand})$ and if this is the case one adds one to the counter $C$. This procedure should be repeated for a large number $N$ of times. For large $N$ the relation

$$\frac{C}{N} = \frac{I}{A} \tag{3.3}$$

holds, where $A$ is the area $A = (x_2 - x_1)f_{max}$. So the value of the integral 3.2 is

$$I = \frac{C}{N}(x_2 - x_1)f_{max} \tag{3.4}$$

In general one does not have to choose $f_{max}$ as the maximum of $f$ but it has to be larger than $f(x)$ for all $x \in (x_1, x_2)$. But the larger one chooses $f_{max}$ the less efficient is the procedure.

## 3.2 Generation of the Hard Process

The hard process of an event contains the collision of two partons of the protons and the creation of new particles out of that. Not included are further decays or interactions of particles. So for example in the $t\bar{t}H$ channel the hard process is only the interaction $pp \to t\bar{t}H$ . In this thesis the event generators aMC@NLO and PowHel are studied.

### 3.2.1 aMC@NLO

aMC@NLO [2] is a fully automatic event generator that is based on the MADGRAPH 5 [23] package. It is able to generate any kind of event at LO and furthermore aMC@NLO includes QCD corrections for Standard Model processes with NLO accuracy. For the QCD corrections the MADLOOP [24] [25] and MADFKS [26] package are used. In addition to Standard Model processes also beyond the Standard Model physics such as interactions with supersymmetric particles can be simulated. To include spin correlations and off shell corrections of decaying or produced particles one can use Madspin [5] (see section 3.3.3).

### 3.2.2 PowHel

Powhel [1] is an event generator that can simulate events and compute cross sections at NLO QCD accuracy. For the QCD corrections the HELAC-1LOOP [27] package is used.

## 3.3 Parton Showering and Hadronisation

Parton shower and hadronisation models simulate three kinds of processes:

1. **Decay:** The particles, that were created in the hard process, can decay into new particles. For example the $t$ quarks and the Higgs boson in the $t\bar{t}H$ process.

2. **Parton showering:** Whenever an electrically charged particle is accelerated it emits photons. In a similar way a colour carrying particle emits gluons. But gluons themselves carry a colour. So they radiate off further gluons and a cascade of quarks and gluons occurs in the detector. This radiation can either originate from the partons before the collision (initial state radiation) or from quarks and gluons that are created in the collision (final state radiation).

3. **Hadronisation:** Particles that carry a colour are never observed separately. They form colourless bound states in a process that is called hadronisation. This hadronisation can be simulated with two different models: The string model and the cluster model.

Here the models Herwig++ and Pythia 8 are used and compared.

### 3.3.1 Pythia 8

Pythia 8 [3] is based on C++ and uses the Lund string model for the modeling of the hadronisation process. For the underlying event a multiple interaction model has been developed. Pythia 8 is based on dipole showering.

#### String Model

If two colour connected quarks are traveling in different directions the strong force is attractive and the potential energy increases with the distance between the quarks. Because of the self attraction of gluons, one can think of the exchanging gluons to collapse into a string or fine tube between the two initial quarks.
When the potential energy is large enough it is energetically favourable for the string to split into two quarks. Each pairs with one initial quark forming a bound state. This procedure continuous until the potential energy between two quarks is not large enough anymore to create a pair of quarks.
The situation becomes more complex if there are more than two particles. In that case each parton has a partner connected via a string segment. Consider for example two

quarks and a gluon. In that case each quark has one string connection with the gluon. The comparison of this scenario with for example a situation with two quarks and photon yields an interesting observation. When the showering happens one expects (and that is what is measured) less jets between the quarks and more jets between the quarks and the gluon. In case of two quarks and a photon one observes more jets in the space between the quarks. This observation is known under the name string effect.

### 3.3.2 HERWIG++

HERWIG++ [4] is based on angle ordered parton showers. The hadronisation model which is used here is a cluster model and for the underlying event HERWIG++ is interfaced to JIMMY [28].

#### Cluster Model

In the cluster model partons with much less energy than the energy of the hard process form colourless groups. These groups or clusters are also called proto-hadrons that decay into the hadrons which then are measured in the detector. At a hadronisation scale of $Q_0 \approx 1\,\text{GeV}$ most clusters have less energy than $3\,\text{GeV}$. This limits the transverse momentum of the decay products of the clusters.

### 3.3.3 Madspin

The Madspin algorithm [5] is implemented in the MADGRAPH 5 framework and can therefore be used together with aMC@NLO. Madspin is used to decay heavy resonances such as the top quark.
The decay of heavy resonances at NLO is very challenging because often the decay products are not stable but decay further. This leads to a large jet multiplicity in the final state that depends strongly on how the initial heavy resonance decayed.
The parton shower models can do these decays as well. However, in some cases this is a bit inaccurate because spin correlation effect and off shell mass effects may both be modelled properly. They use the narrow width approximation, where the intermediate particles are put on their mass shells. The result of this is that radiation effects before and after the interaction can be treated separately. The narrow width approximation is a good choice, if the decay rate $\Gamma$ is small compared to the mass $m$.
To take off shell effects into account, in the Madspin algorithm the mass of intermediate particles is smeared out with a Breit-Wigner distribution. This means one may have to alter the momentum of the undecayed particles and because of momentum conservation

also the momentum of the decay products. This process is called momentum reshuffling. In addition, in contrast to parton shower models, the Madspin algorithm includes spin correlation effects.

## 3.4 Detector Simulation

In detector simulations the signal of the detector is simulated. In general a detector is a very complex structure with many layers and materials. So it is very challenging to simulate the whole signal of a detector like the ATLAS detector. Due to this complexity in this thesis no detector simulations are performed. An example of a detector simulator is GEANT [29].

# 4 Generation of $t\bar{t}H$ Samples

This chapter describes how the datasets were produced. Here it is important which inputs were necessary and how the paramters were chosen.

## 4.1 Hard Process Generation

With the aMC@NLO generator at least one million $t\bar{t}H$ events at a center of mass energy of $\sqrt{s} = 8\,\text{TeV}$ for each dataset were produced at NLO accuracy. The events are inclusive in top quark and Higgs boson decay. As PDF set CT10NLO was used. The renormalisation scale and factorisation scale were equally chosen dynamically to $\mu_R = \mu_F = (m_T^H + m_T^t + m_T^{\bar{t}})/2$. The mass of the top quark was set to 172.5 GeV and the mass of the Higgs boson to 125 GeV.
The output of the aMC@NLO program are LHE files [30], which can be used as input for the parton shower simulations. In LHE files all events are listed in text form. The MADGRAPH 5 framework, in which aMC@NLO runs, also has an option to run Madspin to decay the top quark.
The official PowHel samples here have been studied and compared with the generated aMC@NLO samples. The same PDF set and values for $m_t$ and $m_H$ have been used while in this case static scales were used $\mu_F = \mu_R = (m_t + m_H)/2$.

## 4.2 Parton Showering and Hadronisation

For the parton showering and hadronisation HERWIG++ and PYTHIA 8 were used. It is possible to select either the hard process data or the after showering data from a dataset. The hard process particles can be distinguished from the after shower particles with status codes. In a PYTHIA 8 file the following status codes have the meaning:

- mc_status= 21-29 : Hard process particle
- mc_status = 61-69 Particles produced by beam-remnant treatment

Figure 4.1 shows an extract of the output of the selection code for a PYTHIA 8 $t\bar{t}H$ event. Based on this it is possible to trace back the development of the event. To analyse the hard process, particles with the status codes 21-29 were chosen and to analyse after showering particles, the status codes 61-69 were chosen.
In HERWIG++ the status code of all particles is 11. So here the parantIdx and childIdx were used to distinguish between hard process and showered particles.

```
***** NEW EVENT *****
Before classifying LEPTON+JETS...
Before loop over MC particles (size: 86)
MC particle: 0 with barcode 5, PDGid 25, status 22 with parentPDG -1000 and parentIdx -1000 & childPDG 25 and childIdx 3
MC particle: 1 with barcode 6, PDGid 6, status 22 with parentPDG -1000 and parentIdx -1000 & childPDG 6 and childIdx 4
MC particle: 2 with barcode 7, PDGid -6, status 22 with parentPDG -1000 and parentIdx -1000 & childPDG -6 and childIdx 5
MC particle: 3 with barcode 10, PDGid 25, status 44 with parentPDG 25 and parentIdx 0 & childPDG 25 and childIdx 6
MC particle: 4 with barcode 11, PDGid 6, status 44 with parentPDG 6 and parentIdx 1 & childPDG 6 and childIdx 7
MC particle: 5 with barcode 12, PDGid -6, status 44 with parentPDG -6 and parentIdx 2 & childPDG -6 and childIdx 8
MC particle: 6 with barcode 16, PDGid 25, status 44 with parentPDG 25 and parentIdx 3 & childPDG 25 and childIdx 9
MC particle: 7 with barcode 17, PDGid 6, status 44 with parentPDG 6 and parentIdx 4 & childPDG 6 and childIdx 10
MC particle: 8 with barcode 18, PDGid -6, status 44 with parentPDG -6 and parentIdx 5 & childPDG -6 and childIdx 11
MC particle: 9 with barcode 23, PDGid 25, status 44 with parentPDG 25 and parentIdx 6 & childPDG 25 and childIdx 12
MC particle: 10 with barcode 24, PDGid 6, status 44 with parentPDG 6 and parentIdx 7 & childPDG 6 and childIdx 13

...

MC particle: 57 with barcode 1129, PDGid 5, status 23 with parentPDG 6 and parentIdx 55 & childPDG -1000 and childIdx -1000
 INFO bquarkfromTop:     57
MC particle: 58 with barcode 1130, PDGid 24, status 22 with parentPDG 6 and parentIdx 55 & childPDG 2 and childIdx 61
 INFO WplusfromTop:     58
MC particle: 59 with barcode 1131, PDGid -5, status 23 with parentPDG -6 and parentIdx 56 & childPDG -1000 and childIdx -1000
 INFO bbarquarkfromTbar:     59
MC particle: 60 with barcode 1132, PDGid -24, status 22 with parentPDG -6 and parentIdx 56 & childPDG -16 and childIdx 63
 INFO WminusfromTbar:     60
MC particle: 61 with barcode 1133, PDGid 2, status 23 with parentPDG 24 and parentIdx 58 & childPDG -1000 and childIdx -1000
 INFO QfromWplus:     61
UpfromWplus 1
MC particle: 62 with barcode 1134, PDGid -1, status 23 with parentPDG 24 and parentIdx 58 & childPDG -1000 and childIdx -1000
 INFO QbarfromWplus:     62
Downbarfromwplus 1
MC particle: 63 with barcode 1183, PDGid -16, status 1 with parentPDG -24 and parentIdx 60 & childPDG -1000 and childIdx -1000
 INFO antineutrino:     63
MC particle: 64 with barcode 1184, PDGid 15, status 2 with parentPDG -24 and parentIdx 60 & childPDG 16 and childIdx 67
 INFO lminusfromwminus:     64
taufromwminus 1/ leptfromwminus 1
MC particle: 65 with barcode 1185, PDGid 5, status 23 with parentPDG 25 and parentIdx 54 & childPDG -1000 and childIdx -1000
INFO HIGGS decay to b:     65
MC particle: 66 with barcode 1186, PDGid -5, status 23 with parentPDG 25 and parentIdx 54 & childPDG -1000 and childIdx -1000
INFO HIGGS decay to bbar:     66

...
```

***Figure 4.1:*** Extract of the output of the selection code for a PYTHIA 8 $t\bar{t}H$ event. In the first paragraph the Higgs boson (PDGid=25), the top quark (PDGid=6) and the anti top quark (PDGid=-6) do not decay. In the second paragraph these particles decay as expected in the $\ell + jets$ channel.

## 4.3 Studied Datasets

In total five different datasets with a center of mass energy of $\sqrt{s} = 8\,\text{TeV}$ were compared:

1. PowHel + PYTHIA 8 (∼1M events)
2. aMC@NLO + PYTHIA 8 (∼ 0.36M events)
3. aMC@NLO + Madspin + PYTHIA 8 (∼ 0.36M events)
4. aMC@NLO + HERWIG++ (∼ 1.8M events)
5. aMC@NLO + Madspin + HERWIG++ (∼ 1.8M events)

The number of events quoted, is before the $H \to b\bar{b}$ cut has been applied. According to the branching ratio (see table 2.1) the Higgs boson decays into $b\bar{b}$ in 58% of the events. The $\ell + \ jets$ cut has been applied in all cases.

# 5 Results

In this chapter the results are presented. All plots are normalised to unity so that the number of events does not affect the comparisons itself. However, there might be statistical uncertainties in bins with only a few events.
Before the actual analysis the used variables are defined:

- $p_T(X)$: Transverse momentum of particle X
- $\eta(X)$: Pseudorapidity of particle X
- $N_{jets}(p_T > 25\,\text{GeV})$: Number of jets with $p_T > 25\,\text{GeV}$ and $|\eta| < 2.5$
- $H_T^{jets}(p_j > 25)$: Total $p_T$ of all jets with $p_T > 25\,\text{GeV}$ and $|\eta| < 2.5$
- $p_T(jj)_{maxPt}$: Sum of transverse momenta of the dijet system with maximum $p_T$
- $dRjj_{maxPt}$: Distance between the two jets with maximum $p_T$
- $dRjj_{mindR}$: Minimum distance between two jets
- $mjj_{maxPt}$: Mass of the dijet system with maximum $p_T$
- $mjj_{mindR}$: Mass of the dijet system with the minimum angle in between

The jets have been reconstructed with the Anti-k(t) jet clustering algorithm [31] with a radius parameter $R = 0.4$.

## 5.1 Comparison of PowHel and aMc@nlo

The first comparison is the comparison of the event generators PowHel and aMc@nlo. These generators have been studied at hard process level and after showering the events with Pythia 8. The PowHel datasets have been produced with a static scale whereas the aMc@nlo datasets have been produced with a dynamic scale. However, the influence of the two different scale choices is small [32].

### 5.1.1 Hard Process

The plots for this comparison can be found in figure 5.1.
The transverse momentum of the top quark (figure: 5.1(a)) and the pseudorapidity (5.1(b)) are similar in both simulations. For the anti top the results are the same. But when looking at the $t\bar{t}$ system (5.1(c) and 5.1(d)) there are significant deviations. The transverse momentum of the $t\bar{t}$ system simulated by PowHel is higher in average. One could assume that because of that the third produced particle, the Higgs boson, carries a different amount of momentum in both simulations. But this is not the case. The comparisons of transverse momentum (5.1(e)) and pseudorapidity of the Higgs boson show no significant differences. When looking at the transverse momentum of the whole $t\bar{t}H$ system (5.1(f)) one can see that in the aMc@nlo simulation in the hard process the total transverse momentum of the system is essentially zero for all events. But in case of the PowHel simulation the momentum is smeared out. So because of momentum conservation there must be other participants in this reaction. As one can see in figure 5.2(f) at least for high values the transverse momenta seem to agree after the showering process. Here both distributions are smeared out due to initial and final state radiation. So the reason might be that PowHel already calculates first radiation emissions for a proper matching to parton shower models.

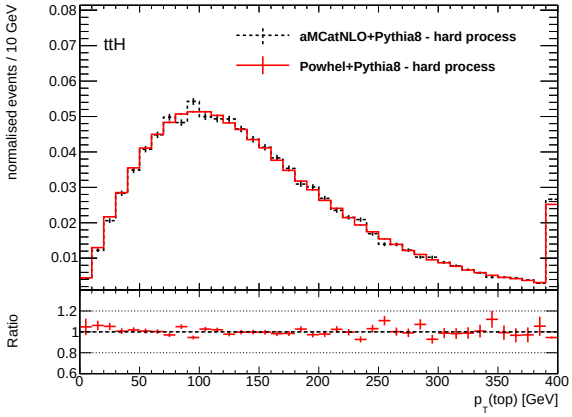


(a) Transverse momentum of the top quark.

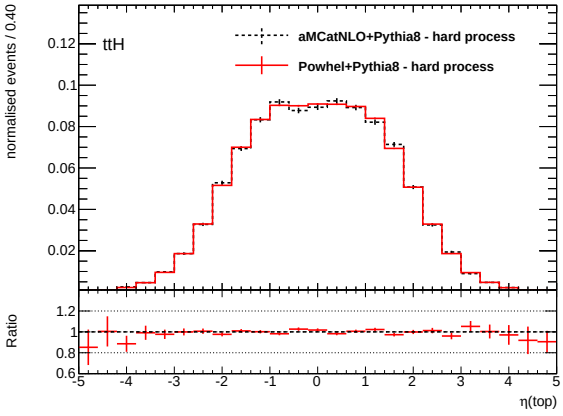


(b) Pseudorapidity of the top quark.

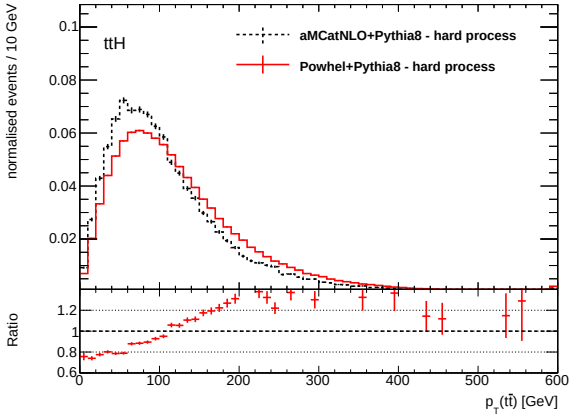


(c) Transverse momentum of the $t\bar{t}$ system.

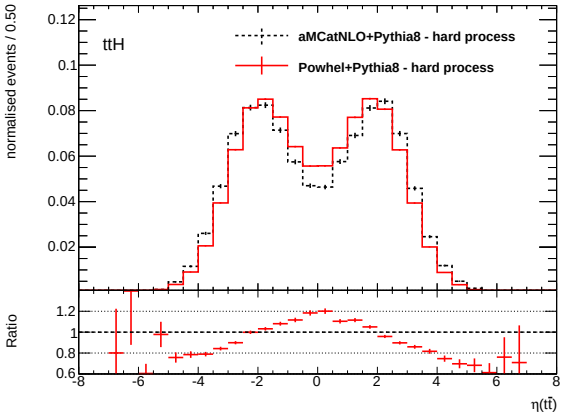


(d) Pseudorapidity of the $t\bar{t}$ system.

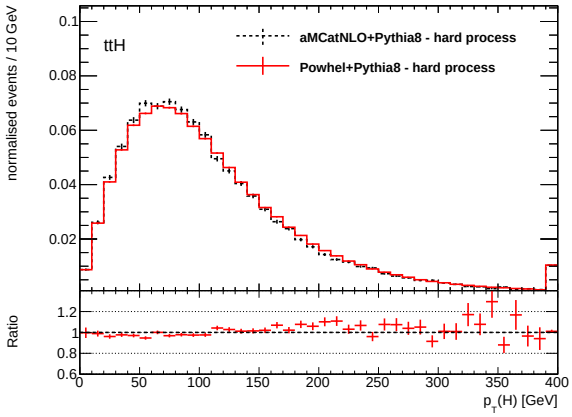


(e) Transverse momentum of the Higgs boson.

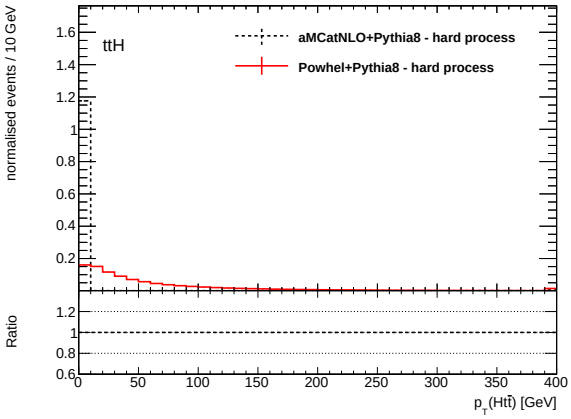


(f) Transverse momentum of the $t\bar{t}H$ system.

***Figure 5.1:*** Comparison plots for the hard process events of PowHel and aMc@nlo.

### 5.1.2 After Showering

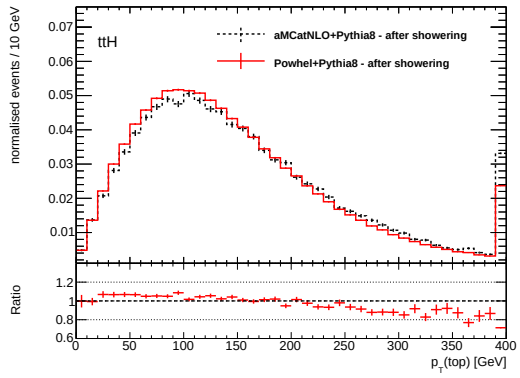


(a) Transverse momentum of the top quark.

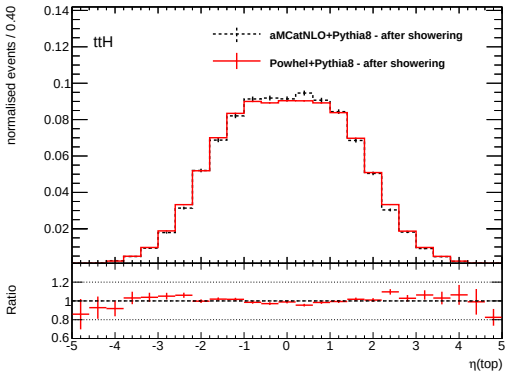


(b) Pseudorapidity of the top quark.

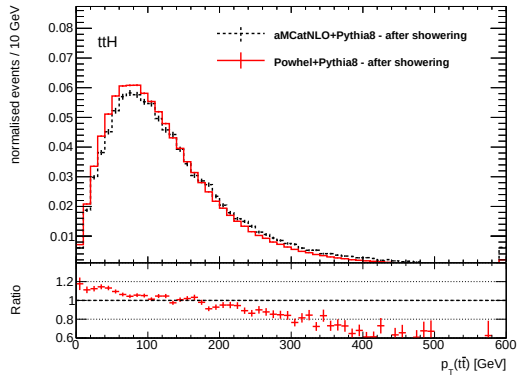


(c) Transverse momentum of the $t\bar{t}$ system.

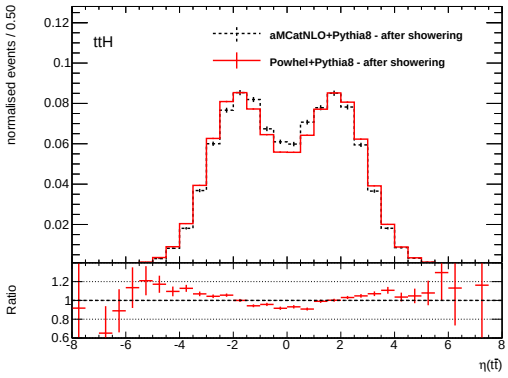


(d) Pseudorapidity of the $t\bar{t}$ system.

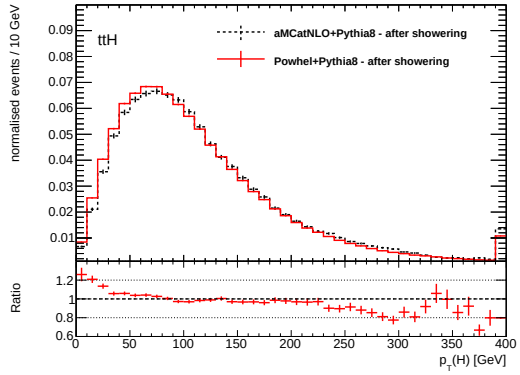


(e) Transverse momentum of the Higgs boson.

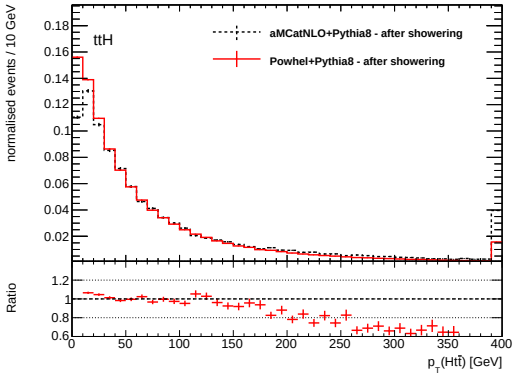


(f) Transverse momentum of the $t\bar{t}H$ system.

***Figure 5.2:*** Comparison plots of PowHel and aMc@nlo after the showering.

The comparison after showering can be found in the figures 5.2, 5.3 and A.1 in the appendix.
After the showering process the transverse momentum and pseudorapidity of the $t\bar{t}$ system have approached. In fact, now the aMC@NLO generated $t\bar{t}$ systems seem to be more energetic (5.2(c)) and more centered (5.2(d)).
The events, that were generated by aMC@NLO tend to have more jets than PowHel events (5.3(a)). Also the jets in aMC@NLO events on average have more transverse momentum (5.3(b)) what is also supported by the comparison of the two jets with the highest transverse momentum (5.3(c)). But the distance between these two jets is similar (5.3(d)).
Because of the different properties in the showering variables, there seems to be a difference how PowHel and aMC@NLO prepare the events for parton shower models.

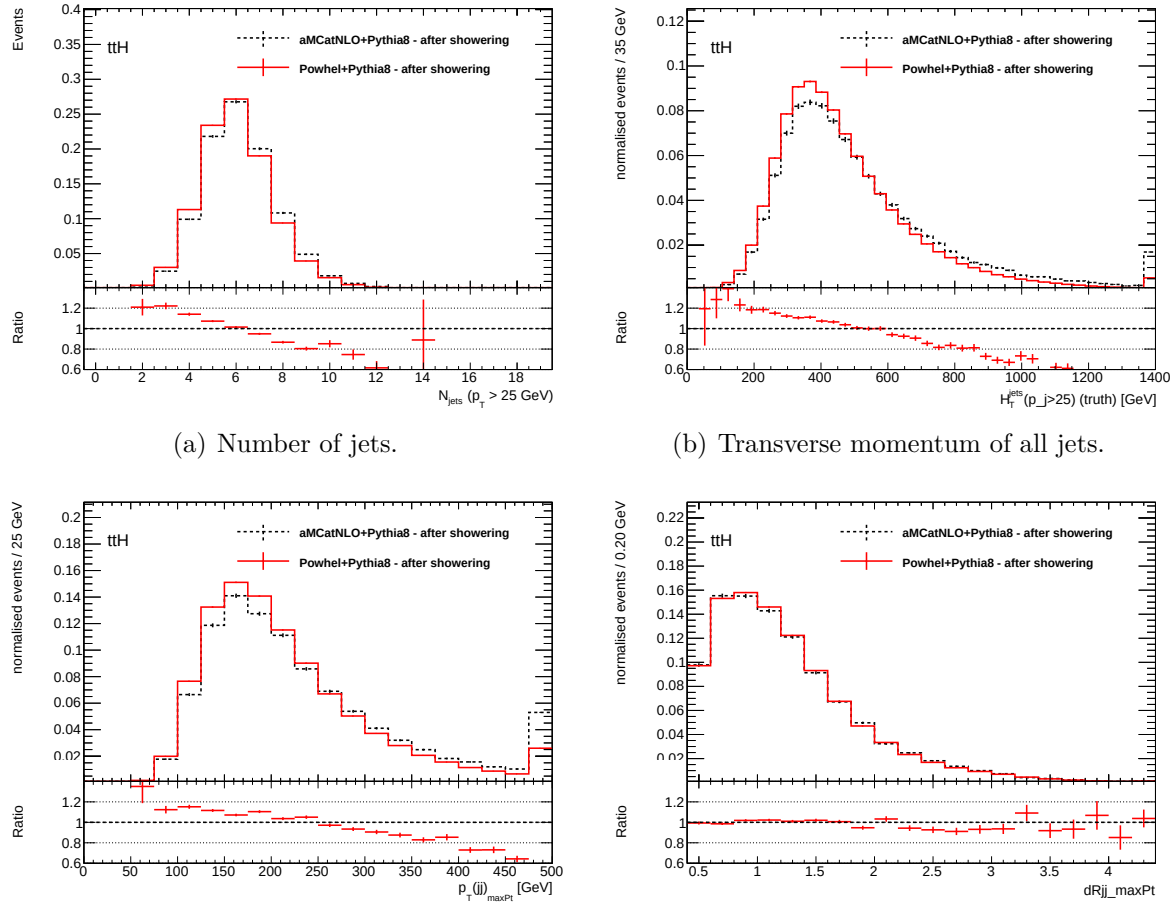


(a) Number of jets.

(b) Transverse momentum of all jets.

(c) $p_T$ of the two jets with highest $p_T$.

(d) Distance between the jets with highest $p_T$.

***Figure 5.3:*** Comparison plots of PowHel and aMC@NLO after the showering.

## 5.2 The Effect of Madspin

The decay of heavy resonances such as the top quarks can be simulated either by Madspin or by the parton shower models. So to analyse the effect of Madspin, datasets with and without this package have been compared. The comparisons have been done for the two parton shower models Pythia 8 and Herwig++.
The interesting variables here are obviously the kinematic variables of the decay products of the top quark.

### 5.2.1 Pythia 8

The plots belonging to this comparison can be found in figure 5.4.
The b quarks in the plots originate from top quark. But in $p_T$ and $\eta$ of the b quarks (5.4(a) and 5.4(b)) no significant deviations are visible. In the same manner the lepton $p_T$ and $\eta$ (5.4(e),5.4(f)) show only small differences and also $p_T$ and $\eta$ of the $W^-$ boson (5.4(c),5.4(d)) agree in both simulations.
So in these variables Madspin does not seem to improve the accuracy of heavy resonance decays.

### 5.2.2 Herwig++

The results of the comparison of the top quark decayed by Madspin or Herwig++ are in figure A.2 in the appendix. The analysed variables are the same as in the Pythia 8 case.
As in the Pythia 8 comparison, in none of the analysed variables a significant deviation was observable.

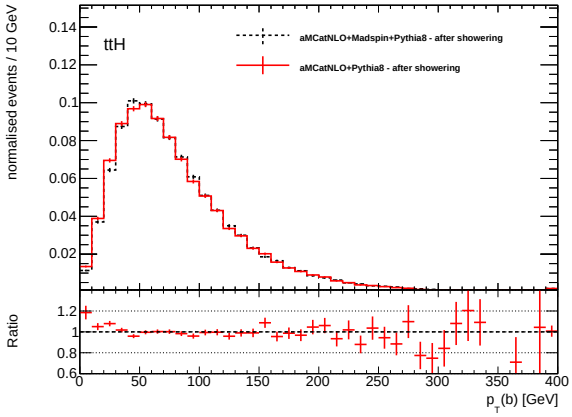


(a) Transverse momentum of the b quark.

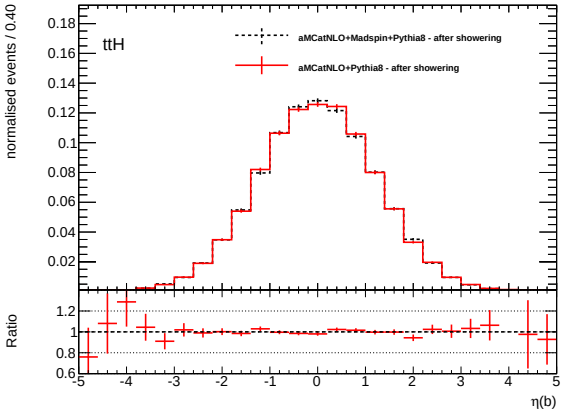


(b) Pseudorapidity of the b quark.

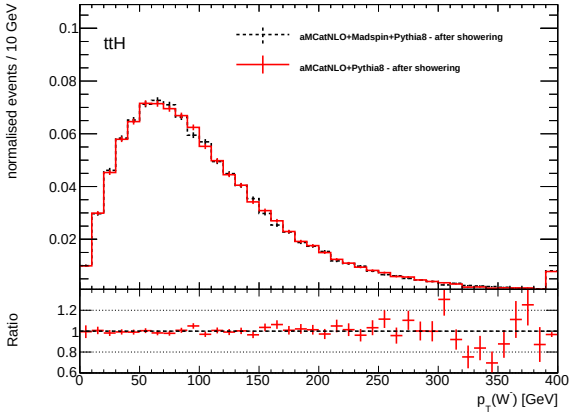


(c) Transverse momentum of the $W^-$ boson.

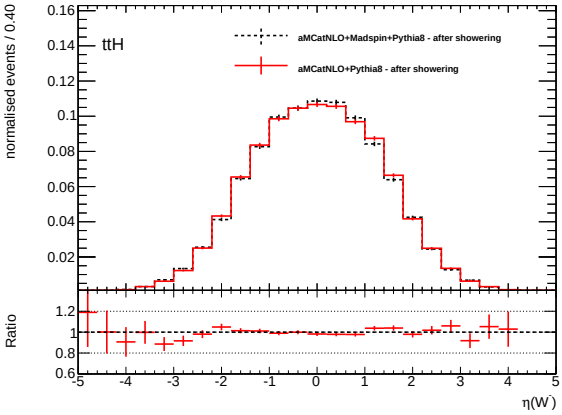


(d) Pseudorapidity of the $W^-$ boson.

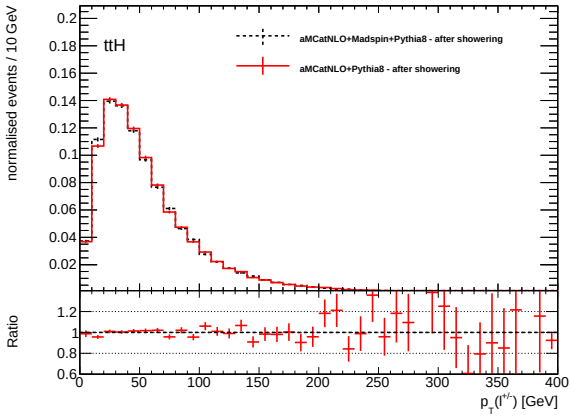


(e) Transverse momentum the leptons.

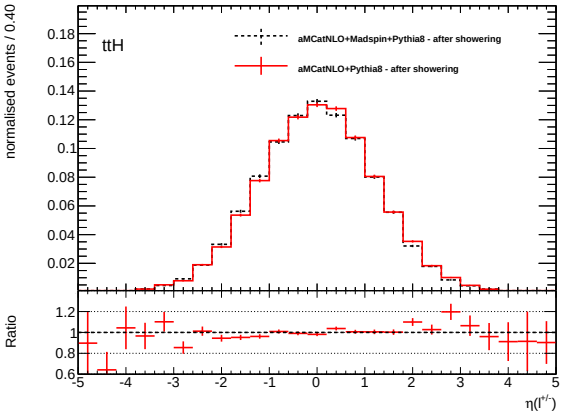


(f) Pseudorapidity of leptons.

***Figure 5.4:*** Comparison plots of PYTHIA 8 datasets with and without Madspin.

## 5.3 Comparison of Pythia 8 and Herwig++

Finally, the parton shower models Pythia 8 and Herwig++ are compared. First they are compared without Madspin and then with Madspin. In both cases the comparison was made after the showering.
The results of Pythia 8 and Herwig++ may differ because Pythia 8 uses the string model (see section 3.3.1) for hadronisation while Herwig++ uses the cluster model (see section 3.3.2).

### 5.3.1 Without Madspin

The plots in the figures 5.5, 5.6 and A.3 belong to this comparison.
The $p_T$(top) distribution of Pythia 8 (5.5(a)) seems to be slightly shifted towards higher transverse momenta. However, this deviations are smaller than 10% in the ratio. The result of the anti top quark and the Higgs boson shows the same behaviour which leads to relatively large deviations in the $t\bar{t}H$ system (5.5(e)). Here the data differs by more than 20% in some bins and clearly a linear slope is observable in the ratio plot.
The results for the pseudorapidity of the particles and systems (5.5(b), 5.5(d) and 5.5(f)) are the same. Whenever $p_T$ in the Herwig++ simulation tends to be smaller, the pseudorapidity curve is broader.
Deviations in the shower variables are expected. Interesting are for example the number of jets with more than 25 GeV (5.6(a)) and the total transverse momentum of jets with more than 25 GeV (5.6(b)). Herwig++ seems to simulate the showering with less jets and these jets also tend to have less transverse momentum. The cause of this is probably the different hadronisation models. It is plausible for Herwig++ to have less jets since it uses the cluster model. If the quarks and gluons build clusters there are less of them then mesons in the string model. The statement that the Herwig++ jets have on average less momentum is also supported by the plot 5.6(c) and also they are lighter (5.6(d)).
The comparisons of the transverse momenta of b quarks (A.3(a) in the appendix), $W^+$ bosons (A.3(c)) and leptons (A.3(e)) yield no remarkable differences. The same holds for the rapidities (A.3(b), A.3(f), A.3(d)).

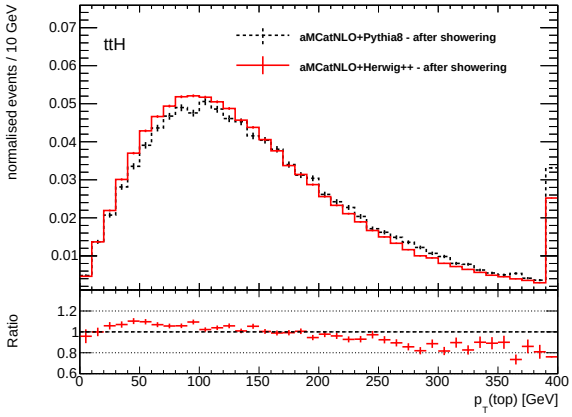


(a) Transverse momentum of the top quark.

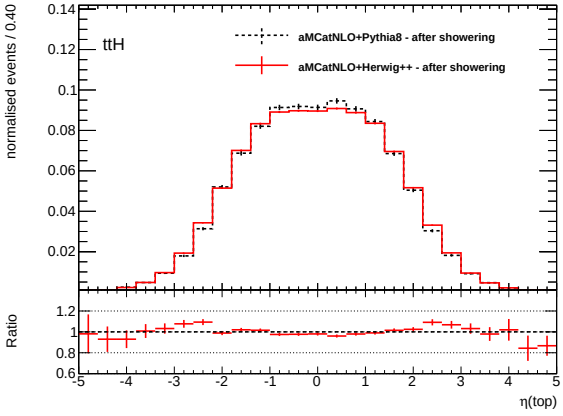


(b) Pseudorapidity of the top quark.

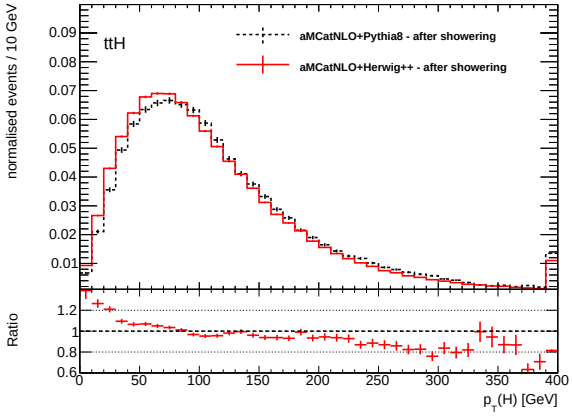


(c) Transverse momentum of the Higgs boson.

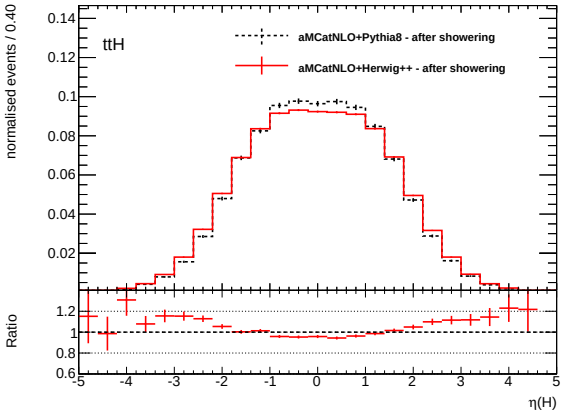


(d) Pseudorapidity of the Higgs boson.

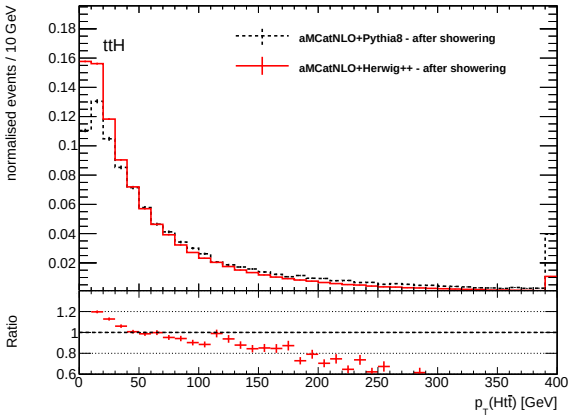


(e) Transverse momentum of the $t\bar{t}H$ system.

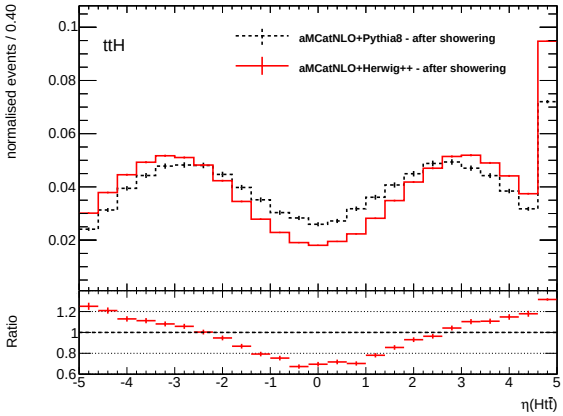


(f) Pseudorapidity of the $t\bar{t}H$ system.

***Figure 5.5:*** Comparison plots of PYTHIA 8 and HERWIG++ datasets without Madspin.

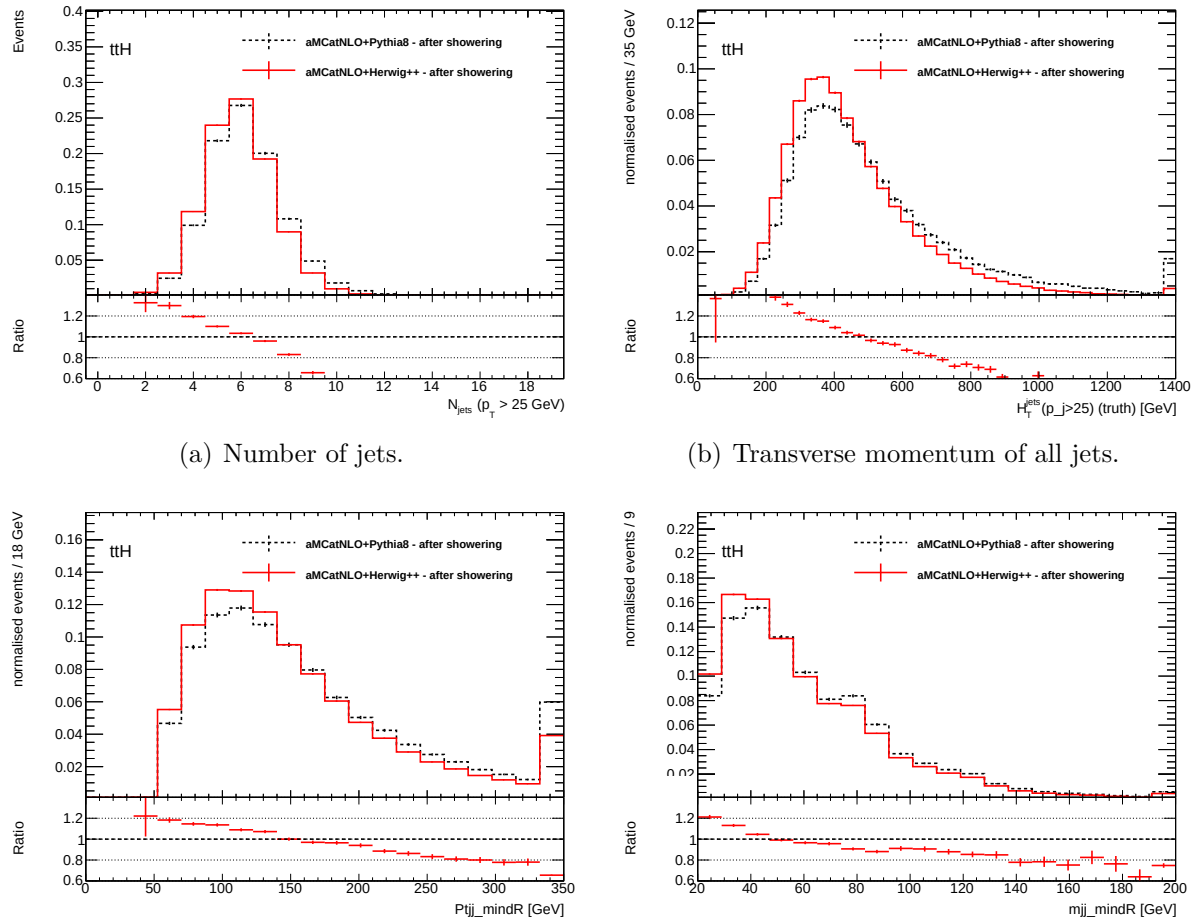


(a) Number of jets.

(b) Transverse momentum of all jets.

(c) $p_T$ of the two closest jets.

(d) Mass of the two closest jets.

***Figure 5.6:*** Comparison plots of PYTHIA 8 and HERWIG++ datasets without Madspin.

### 5.3.2 With Madspin

The comparison of PYTHIA 8 and HERWIG++ with Madspin can be found figure A.4 in the appendix.

As the comparison of Madspin datasets with no Madspin datasets in section 5.2 yielded no essential differences, it is not surprising that the results here are the same as in the section before (5.3.1).

# 6 Conclusion

In this bachelor thesis in total more than four million $t\bar{t}H$ events have been generated with the aMC@NLO generator. This has not been done before because aMC@NLO is a relatively new program. This is also the reason why it is important to study its properties. The generation took a long time because first I had to learn about status codes and how to select the properties of particles in the hard process or after showering. To generate such a large number of events it was necessary to run the parton showering on the grid, which has some difficulties.

The comparison with PowHel showed that PowHel events on average are harder than aMC@NLO events.
Furthermore, the effect of Madspin has been studied. The results of the analysed variables showed no differences for datasets with and without Madspin.
The last comparison showed that PYTHIA 8 events seem to have more jets and these jets are more energetic. In the same manner, the other PYTHIA 8 particles have on average more momentum.

Originally, I planned to compare aMC@NLO events generated with different scales. Unfortunately, I did not have enough time to complete this for the bachelor thesis.

# A Appendix

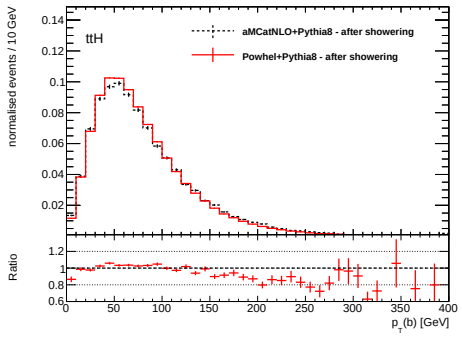


(a) Transverse momentum of the b quark.

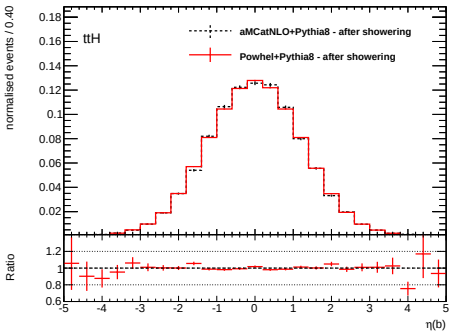


(b) Pseudorapidity of the b quark.

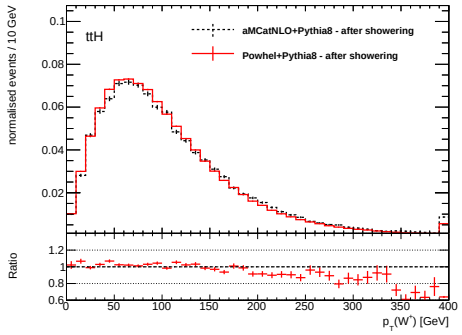


(c) Transverse momentum of the $W^+$ boson.

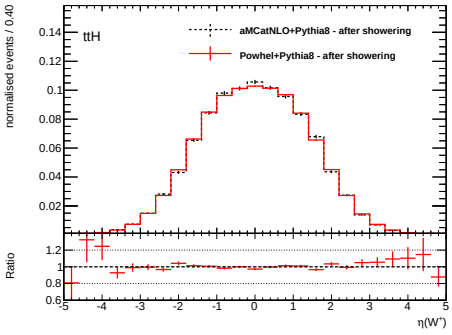


(d) Pseudorapidity of the $W^+$ boson.

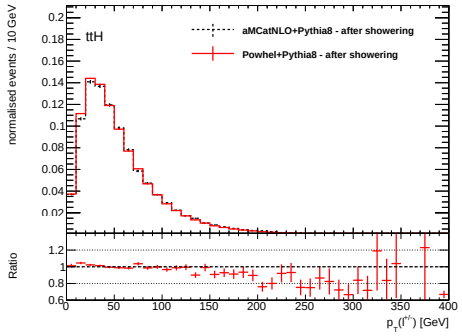


(e) Transverse momentum the leptons.

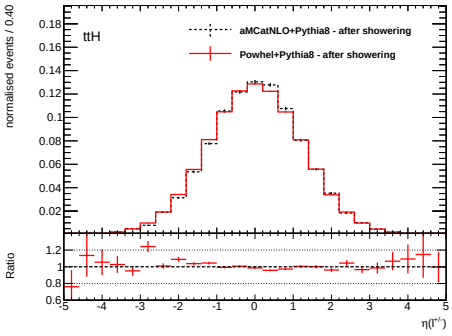


(f) Pseudorapidity of leptons.

***Figure A.1:*** Comparison plots of PowHel and aMC@NLO after the showering.

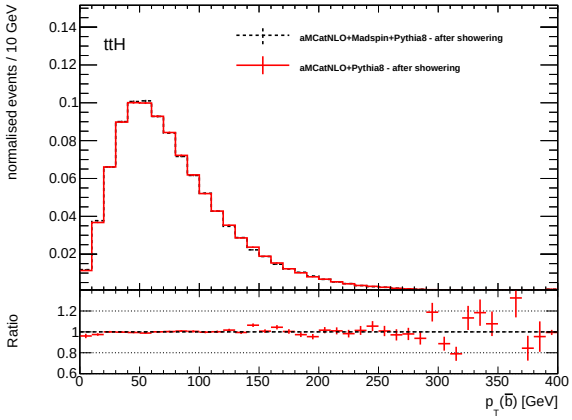


(a) Transverse momentum of the anti b quark.

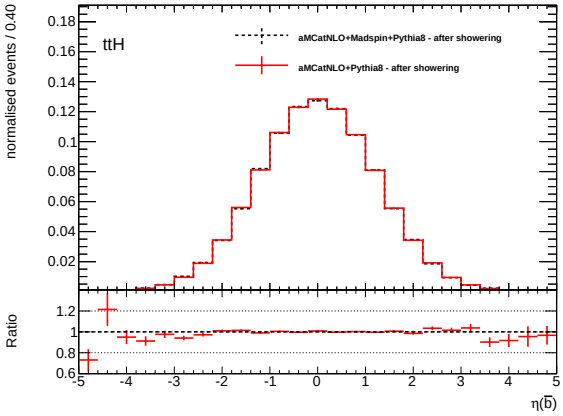


(b) Pseudorapidity of the anti b quark.

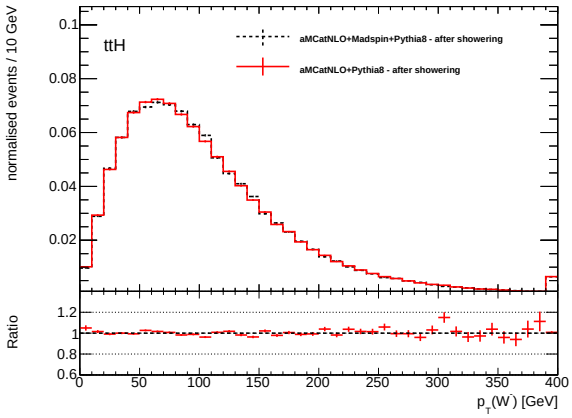


(c) Transverse momentum of the $W^-$ boson.

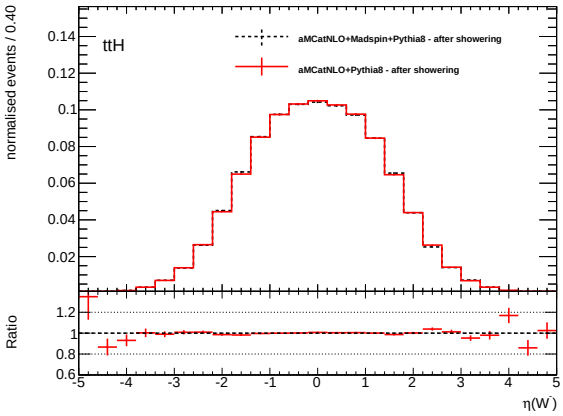


(d) Pseudorapidity of the $W^-$ boson.

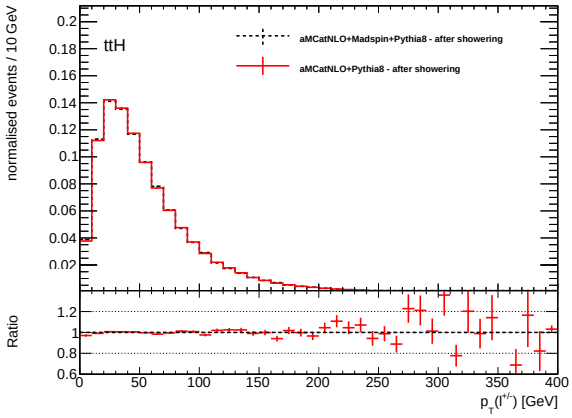


(e) Transverse momentum the leptons.

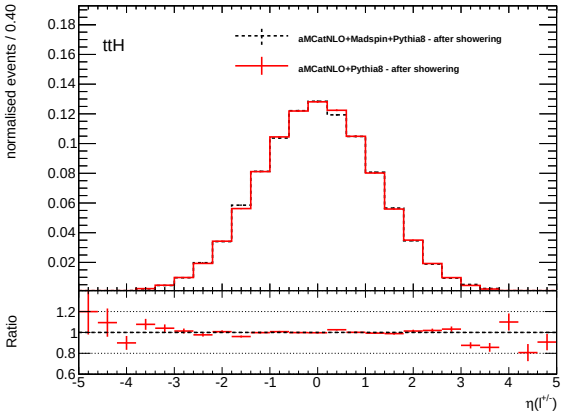


(f) Pseudorapidity of leptons.

***Figure A.2:*** Comparison plots of HERWIG++ datasets with and without Madspin.

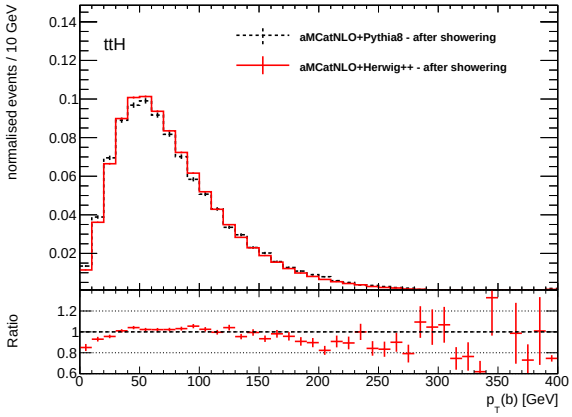


(a) Transverse momentum of the b quark.

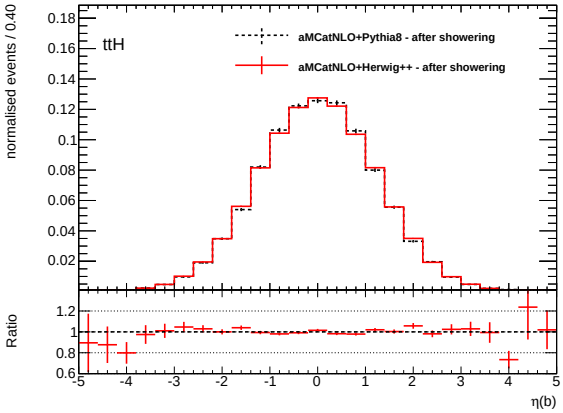


(b) Pseudorapidity of the b quark.

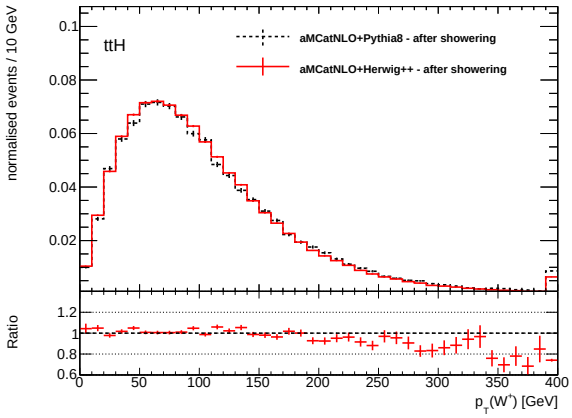


(c) Transverse momentum of the $W^+$ boson.

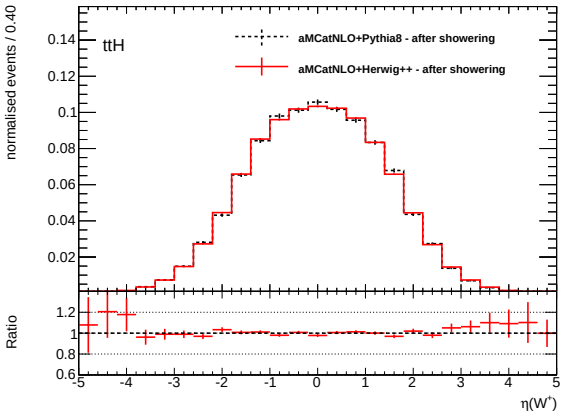


(d) Pseudorapidity of the $W^+$ boson.

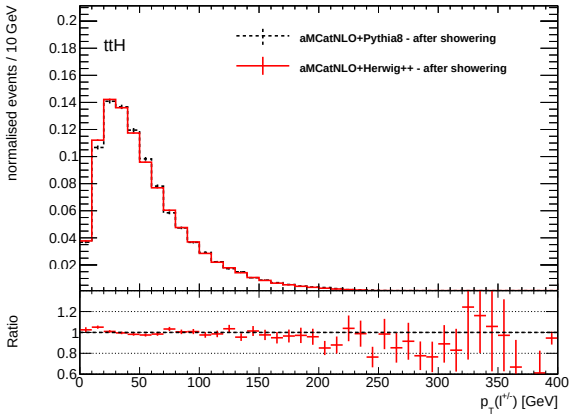


(e) Transverse momentum of leptons.

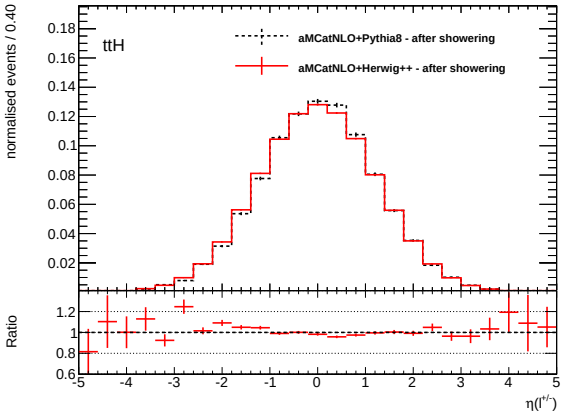


(f) Pseudorapidity of the leptons.

***Figure A.3:*** Comparison plots of PYTHIA 8 and HERWIG++ datasets without Madspin.

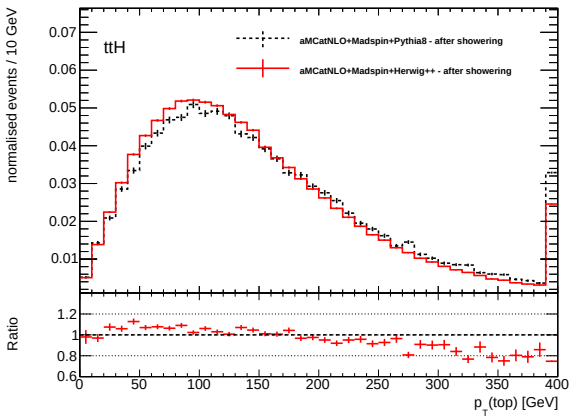


(a) Transverse momentum of the top quark.

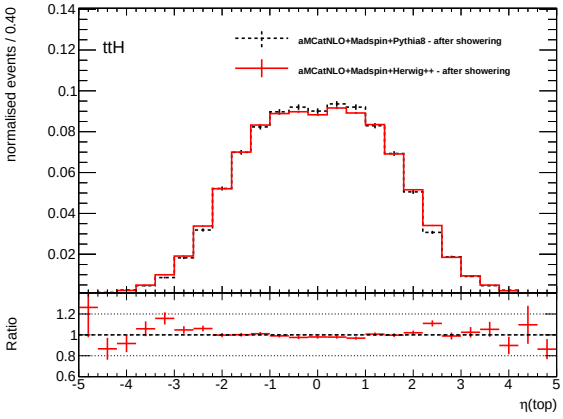


(b) Pseudorapidity of the top quark.

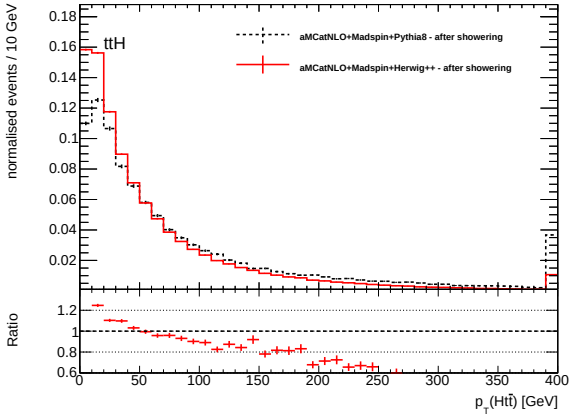


(c) Transverse momentum of the $t\bar{t}H$ system.

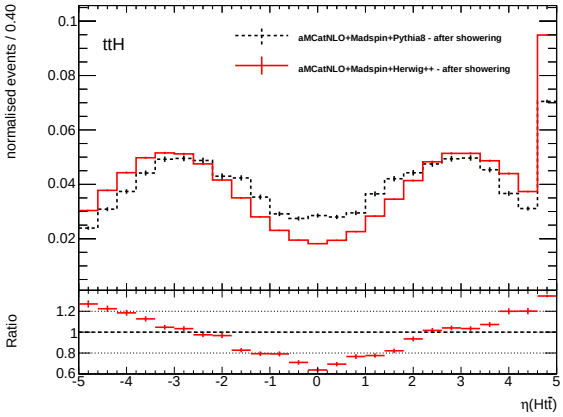


(d) Pseudorapidity of the $t\bar{t}H$ system.

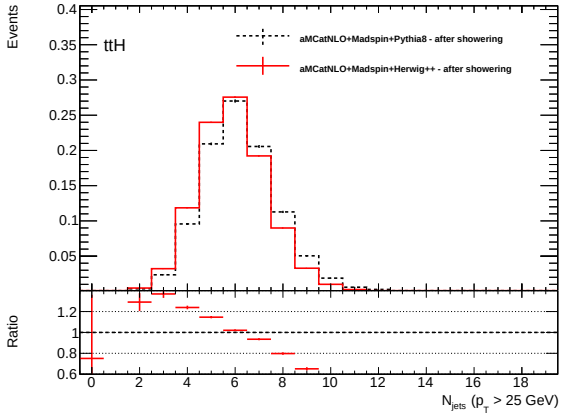


(e) Number of jets.

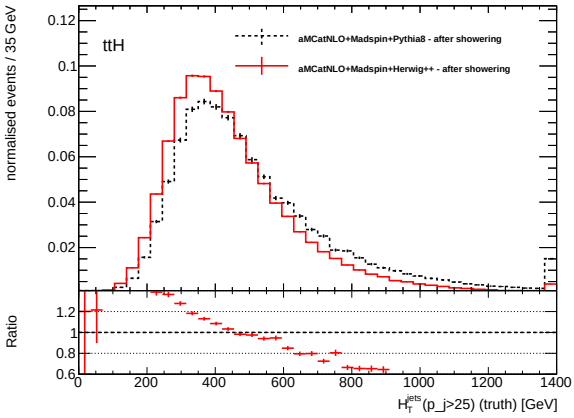


(f) Transverse momentum of all jets.

***Figure A.4:*** Comparison plots of PYTHIA 8 and HERWIG++ datasets with Madspin.

# Bibliography


[1] M. Garzelli, et al., *$t\bar{t}$ pair hadroproduction in association with a heavy boson at the NLO QCD accuracy + Parton Shower*, J.Phys.Conf.Ser. **452**, 012046 (2013)

[2] J. Alwall, et al., *The automated computation of tree-level and next-to-leading order differential cross sections, and their matching to parton shower simulations*, JHEP **1407**, 079 (2014)

[3] T. Sjostrand, et al., *A Brief Introduction to PYTHIA 8.1*, Comput. Phys. Commun. **178**, 852 (2008)

[4] M. Bahr, et al., *Herwig++ Physics and Manual*, Eur.Phys.J. **C58**, 639 (2008)

[5] P. Artoisenet, et al., *Automatic spin-entangled decays of heavy resonances in Monte Carlo simulations*, JHEP **1303**, 015 (2013)

[6] D. Griffiths, *Introduction to Elementary Particles*, Physics textbook (2008)

[7] S. Abachi, et al., *Search for High Mass Top Quark Production in $p\bar{p}$ Collisions at $s$ = 1.8 TeV*, Phys. Rev. Lett. **74**, 2422 (1995)

[8] F. Abe, et al., *Observation of Top Quark Production in $p\bar{p}$ Collisions with the Collider Detector at Fermilab*, Phys. Rev. Lett. **74**, 2626 (1995)

[9] ATLAS Collaboration, CDF Collaboration, CMS Collaboration, D0 Collaboration, *First combination of Tevatron and LHC measurements of the top-quark mass*, ATLAS-CONF-2014-008, CDF-NOTE-11071, CMS-PAS-TOP-13-014, D0-NOTE-6416 (2014)

[10] J. Beringer, et al. (Particle Data Group), *Review of Particle Physics*, Phys. Rev. D **86**, 010001 (2012)

[11] A. Quadt, *Top quark physics at hadron colliders*, EPJC **48**, 835 (2006)

[12] P. W. Higgs, *Broken Symmetries, Massless Particles and Gauge Fields*, Phys. Lett. **12**, 132 (1964)

[13] G. Aad, et al., ATLAS Collaboration, *Observation of an Excess of Events in the Search for the Standard Model Higgs boson with the ATLAS detector at the LHC*, ATLAS-CONF-2012-093 (2012)

[14] S. Chatrchyan, et al., CMS Collaboration, *Observation of a new boson at a mass of 125 GeV with the CMS experiment at the LHC*, Phys. Lett. **B716**, 30 (2012)

[15] S. Chatrchyan, et al., CMS Collaboration, *Precise determination of the mass of the Higgs boson and studies of the compatibility of its couplings with the standard model*, Technical Report CMS-PAS-HIG-14-009, CERN, Geneva (2014)

[16] S. Dittmaier, et al. (LHC Higgs Cross Section Working Group), *Handbook of LHC Higgs Cross Sections: 2. Differential Distributions*, ArXiv e-prints (2012)

[17] S. Dittmaier, et al. (LHC Higgs Cross Section Working Group), *Handbook of LHC Higgs Cross Sections: 1. Inclusive Observables* (2011)

[18] O. S. Brüning, et al., *LHC Design Report*, CERN, Geneva (2004)

[19] *www.cern.ch*

[20] G. Aad, et al., ATLAS Collaboration, *The ATLAS Experiment at the CERN Large Hadron Collider*, JINST **A3**, 8003 (2008)

[21] S. Heinemeyer, et al. (LHC Higgs Cross Section Working Group), *Handbook of LHC Higgs Cross Sections: 3. Higgs Properties* (2013)

[22] G. Bevilacqua, M. Worek, *On the ratio of ttbb and ttjj cross sections at the CERN Large Hadron Collider*, JHEP **1407**, 135 (2014)

[23] J. Alwall, et al., *MadGraph 5 : Going Beyond*, JHEP **1106**, 128 (2011)

[24] V. Hirschi, et al., *Automation of one-loop QCD corrections*, JHEP **1105**, 044 (2011)

[25] R. Pittau, *Status of MadLoop/aMC@NLO*, C11-09-26.5 (2012)

[26] R. Frederix, et al., *Automation of next-to-leading order computations in QCD: The FKS subtraction*, JHEP **0910**, 003 (2009)

[27] G. Bevilacqua, et al., *Helac-NLO*, Comp. Phys. Commun. 184 986 (2013)

[28] J.M. Butterworth, et al., *Multiparton interactions in photoproduction at HERA*, Z.Phys. **C72**, 637 (1996)

[29] R. Brun, F. Carminati, S. Giani, *GEANT Detector Description and Simulation Tool*, CERN-W5013, CERN-W-5013 (1994)

[30] J. Alwall, *A Standard format for Les Houches event files*, Comput. Phys. Commun. **176**, 300 (2007)

[31] M. Cacciari, et al., *The Anti-k(t) jet clustering algorithm*, JHEP **0804**, 063 (2008)

[32] S. Henkelmann, *Signal modelling and corresponding uncertainty studies for the search of the Higgs boson produced in association with a top-quark pair at the ATLAS experiment*, II.Physik-UniGö-MSc-2013/02 (2013)

# Acknowledgement

First of all, I would like to thank Prof. Dr. Arnulf Quadt for giving me the opportunity to write my bachelors thesis in his department and also for being the first referee.
Also I want to thank Dr. Kevin Kröninger for not hesitating to assume the role of the second referee.

My special thanks goes to my daily supervisor Dr. Maria Moreno Llacer, who was very dedicated to help me with my problems. Sometimes even until late in the evening. This thesis was a lot of work for her as well and I am very thankful for all her efforts.

Finally, I want to thank Art Gabriel, Fabian Sohns, Jens Oltmanns and Timo Dreyer, who worked on their bachelor theses during the same period of time. We often worked in the same office room, so that we were able to exchange our thoughts and problems. Especially, I want to express my gratitude to Timo, who worked on a similar topic as mine. I think both of our works profited from that because we helped each other in many situations.

**Erklärung** nach §13(8) der Prüfungsordnung für den Bachelor-Studiengang Physik und den Master-Studiengang Physik an der Universität Göttingen:

Hiermit erkläre ich, dass ich diese Abschlussarbeit selbständig verfasst habe, keine anderen als die angegebenen Quellen und Hilfsmittel benutzt habe und alle Stellen, die wörtlich oder sinngemäß aus veröffentlichten Schriften entnommen wurden, als solche kenntlich gemacht habe.
Darüberhinaus erkläre ich, dass diese Abschlussarbeit nicht, auch nicht auszugsweise, im Rahmen einer nichtbestandenen Prüfung an dieser oder einer anderen Hochschule eingereicht wurde.

Göttingen, den 18. Juli 2014

(Felix Wiebe)